Theses and Dissertations--Mining Engineering

Mining Engineering

2022

Strain Energy Analysis Related To Strata Failure During Caving Operations

Caroline Gerwig
University of Kentucky, cgerwig11@gmail.com
Author ORCID Identifier:
https://orcid.org/0000-0003-2987-944
Digital Object Identifier: https://doi.org/10.13023/etd.2022.436

Right click to open a feedback form in a new tab to let us know how this document benefits you.

STUDENT AGREEMENT:

I represent that my thesis or dissertation and abstract are my original work. Proper attribution has been given to all outside sources. I understand that I am solely responsible for obtaining any needed copyright permissions. I have obtained needed written permission statement(s) from the owner(s) of each third-party copyrighted matter to be included in my work, allowing electronic distribution (if such use is not permitted by the fair use doctrine) which will be submitted to UKnowledge as Additional File.

I hereby grant to The University of Kentucky and its agents the irrevocable, non-exclusive, and royalty-free license to archive and make accessible my work in whole or in part in all forms of media, now or hereafter known. I agree that the document mentioned above may be made available immediately for worldwide access unless an embargo applies.

I retain all other ownership rights to the copyright of my work. I also retain the right to use in future works (such as articles or books) all or part of my work. I understand that I am free to register the copyright to my work.

REVIEW, APPROVAL AND ACCEPTANCE

The document mentioned above has been reviewed and accepted by the student's advisor, on behalf of the advisory committee, and by the Director of Graduate Studies (DGS), on behalf of the program; we verify that this is the final, approved version of the student's thesis including all changes required by the advisory committee. The undersigned agree to abide by the statements above.

<div align="right">

Caroline Gerwig, Student

Dr. Zach Agioutantis, Major Professor

Dr. Jhon Silva, Director of Graduate Studies

</div>

STRAIN ENERGY ANALYSIS RELATED TO
STRATA FAILURE DURING CAVING OPERATIONS

_____

THESIS
_____

A thesis submitted in partial fulfillment of the
requirements for the degree of Master of Science in the
College of Engineering at the University of Kentucky

By

Caroline Gerwig

Lexington, Kentucky

Director: Dr. Zach Agioutantis, Professor of Mining Engineering

Lexington, Kentucky

2022

https://orcid.org/0000-0003-2987-9445

ABSTRACT OF THESIS

STRAIN ENERGY ANALYSIS RELATED TO
STRATA FAILURE DURING CAVING OPERATIONS

For stiff beams that can form over the gob of longwall panels, the potential seismic magnitude of the energy released upon strata caving is estimated. Analytical calculations are used to verify two-dimensional models of longwall roof beams to determine the strain energy and gravitational energy developed, that will then be released to surrounding mine workings. Models are developed using RS2 to model the stress, strain, and deflection along the bottom of the longwall roof beam to calculate gravitational and strain energies.

The total energy is then converted to seismic magnitude. Strain energy was consistently less than gravitational energy, except for beams with heights below 15 m in height. Gravitational energy is shown to be the main driving factor in energy release, except for the beams with low heights. Analyses allow the determination of beam characteristics based on seismic data.

The analysis is then refined using swelling factor to compare various beam drop heights. The models show an increase in seismic magnitude for higher drop heights. However, the actual data provided by Buchanan mine displays a decrease in seismic magnitude with increasing drop height, indicating that energy is dissipated into the broken gob material as drop height increases.

KEYWORDS: Longwall roof beams, strain energy, gravitational energy, seismicity

Caroline Gerwig
Name of Student

12/01/2022
Date

STRAIN ENERGY ANALYSIS RELATED TO
STRATA FAILURE DURING CAVING OPERATIONS

By
Caroline Gerwig

Dr. Zach Agioutantis
Director of Thesis

Dr. Jhon Silva
Director of Graduate Studies

12/01/2022
Date

DEDICATION

To my family, and friends who supported me in my academic pursuits. To Laura Letellier who inspired me to continue my formal education, my mom, Lauren, Katie, and Daisy.

ACKNOWLEDGMENTS

TABLE OF CONTENTS

LIST OF TABLES

LIST OF FIGURES

CHAPTER 1. INTRODUCTION

In longwall mining, the progressive caving of the roof strata is essential to the safe operation of the longwall panel. Roof caving following the progression of the shearer relieves stresses and prevents unstable roof conditions from developing. However, in some cases, the roof above a longwall is strong enough that it does not cave progressively with the movement of the panel. Instead, a stiff, unstable beam forms above the open gob. Upon mining of the following panel, it has been found that the beam often fails, releasing a significant amount of seismic energy to the surrounding mine workings.

Before failure, the beam undergoes beam bending. This process stores energy in the form of elastic strain energy. In addition, the beam stores gravitational potential energy by hovering over the open void, with the potential to drop a large weight the distance of the opening. Upon beam failure, these energies are released into the mine. When the beam eventually fails, the stored gravitational and strain energy is released to the surrounding mine workings in the form of seismicity. It is important for the planning of mine operations to be able to estimate the amount of energy released and / or the magnitude of any seismic or microseismic events from these phenomena

In this thesis, the stress and strain of the beam are estimated using a two-dimensional model in order to calculate the strain energy and gravitational energy that will be released upon beam failure. Analytical equations are used to verify the model. A variety of beam properties are tested in order to determine their effect on the released energy. It is assumed that there is bed separation that occurs between the strong beam and the overlying strata. As a result, in this analysis it is assumed that the weight of the overburden does not affect the beam deformation.

It is possible to use the geologic data of the size and location of the failed beam to relate beam dimensions to seismic energy released. The effect of increased drop height, while predicted to increase the seismic magnitude released, in reality decreases seismic magnitude. A cushioning effect by the gob below the beam is potentially the cause of the decreased seismicity.

1

A variety of beam dimensions and properties are shown to affect the seismic magnitude of the energy released due to beam failure. The beam dimensions and drop height are predicted for various potential seismic magnitudes released.

CHAPTER 2. BACKGROUND AND LITERATURE REVIEW

2.1   Literature Review

The progressive collapse of longwall roof strata over the mined-out gob allows for a continuous relief of strain and gravitational energy. Caving of the overlying strata in longwall advancement, along with other large-scale unsupported underground openings, develops a considerable amount of strain energy in the roof strata. In some cases, the overlying strata does not fall progressively as predicted, and the buildup of strain and gravitational energy can produce a sudden, unplanned collapse. Several researchers have proposed methods of modelling this situation using beams or plates to represent the overlying roof strata to estimate stress distribution, deflections, and energy quantities related to these roof strata.

Strong roof beds that do not collapse entirely can bridge or cantilever over the extent of the longwall panel, creating an unstable suspended load. This can lead to an accumulation of large amounts of strain energy in the roof beds and coal seam. The energy will be rapidly released in the event of a roof failure, and can also be rapidly released in the form of coal bursts (Wu & Karfakis, 1993). This latter phenomenon is corroborated by extensive research and documentation of coal bump occurrences in Appalachia and other areas (Goode et al., 1984; Haramy et al., 1987; Iannacchione & DeMarco, 1992).

The release of energy resulting from the failure of the competent structural members is sufficient to cause small-scale seismic events that can be detected by local seismographs (Alber et al., 2008; Choi, 1990; Iannacchione et al., 2005; Luxbacher et al., 1994). Though these earthquakes are not violent enough to pose a danger for surface structures, it is invaluable for mine safety to develop methods for assessing the potential of such phenomena to occur in longwall operations. Efficiently and accurately estimating the capacity and potential of uncontrolled roof caving and failure would allow for effective mine designing and operations scheduling. In this way, productivity of the operations could be increased while at the same time risks of undesired injuries, as well as infrastructure and equipment damage could be minimized.

There are different relative magnitudes of seismic emissions resulting from various failure modes. Cavity collapses, resulting from rock burst in mine roofs extruding a mass

of rock violently down or a mass of rock loosened by mining falling, cause seismic emissions in two forms: from the rock burst and from the pull of gravity. In past studies, rock bursts have been shown to release a greater amount of energy than rock falls. Overall, the most common failure type that occurs overall are edge dislocations and comminuted faults, occurring near the face of open gob. These are caused by a combination of blasting and volume closure (Hasegawa et al., 1989).

A case study performed by Van Dyke et al. (2018) found in a VA longwall mine that sandstone thicknesses of 6-12 m combined with an overburden of about 580 m or greater results in areas where larger seismic events in the range of 1.5 ML or greater were more likely to occur. Furthermore, where these conditions are combined with caving height (distance of the beam from the seam) of 4.6 m or less, there was the highest potential for a large seismic event of 3 ML or greater.

There are multiple calculation methods available for the determination of strain energy development in a member supported on its ends. By altering the assumptions of the model, the energy calculated is altered as well. To compare these energy calculations, the deformation experienced along the roof strata was unified. The estimation of different strain and gravitational energy calculations allows for an approximation of the expected energy release due to sudden failure of the roof.

This thesis compares different methods for calculating the strain energy associated to the phenomenon under investigation. The ultimate objective is to define an approach for efficiently approximating the energy released due to roof caving during longwall development. Energy calculations are derived through the combination of analytical and numerical tools that consider bending of a beam or plate elements. More specifically, a numerical model of the overlying strata is developed which considers the overburden as a bending beam element. The stress and strain calculations derived by that model are combined with analytical methods, both closed form solutions and discrete form solutions, as these are provided from the classical solid body theory. Additionally, the results from the numerical model are compared with an energy approximation approach that is derived by the bending plate element theory.

The stress analysis is conducted under the 2D plane strain assumption, which implies that a slice of a very long panel is modeled. In addition, both models are loaded by

applying the weight of the beam material itself without considering any additional weight from the overburden strata above the beam. This is substantiated by the elastic theory of beams representing stratified roof above underground openings (Pariseau, 2017).

2.2   Background

Several methodologies have been developed from various researchers for calculating the strain energy stored in a material sustaining bending forces. The concept of beam analysis for the description of the strata behavior, under the assumption that these strata can be modeled as ideal, simplified roof formations, uses static and elastic equations to predict the deflection and strain energy developed in these formations. The application of the beam analysis concept in rock-masses and mining operations relies on the simplification of an underground opening to a two-dimensional space, under the assumption that a slice taken of the opening is representative of an infinitely long plate extending along the direction of the opening. The two-dimensional model is assumed to be under plane strain conditions, where the strain in the longitudinal direction is zero, and only the strains in the vertical and horizontal directions are considered.

2.3   Proposed Methodology

Based on the literature review, the proposed methodology for this analysis is described in Figure 2.1. The analysis starts with analytical and numerical modelling of beam deflection. This then allows for the calculation of energy that will be released once the beam caves. On the other side, the seismic monitoring on the part of the mining operation provides data for the event location, strata height, and event magnitude. The energy calculations can then be compared with the event data to determine if there is a significant association between the data.
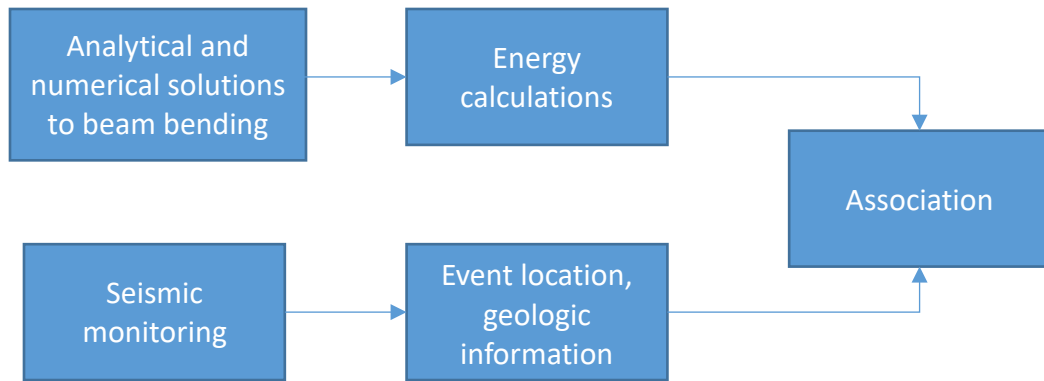
Figure 2.1: Flowchart of proposed methodology

The location being modelled is a beam that forms overtop the gob of a longwall panel, as shown in Figure 2.2. The roof beam is shown in blue and is modelled as a cross-section of the entire panel width.
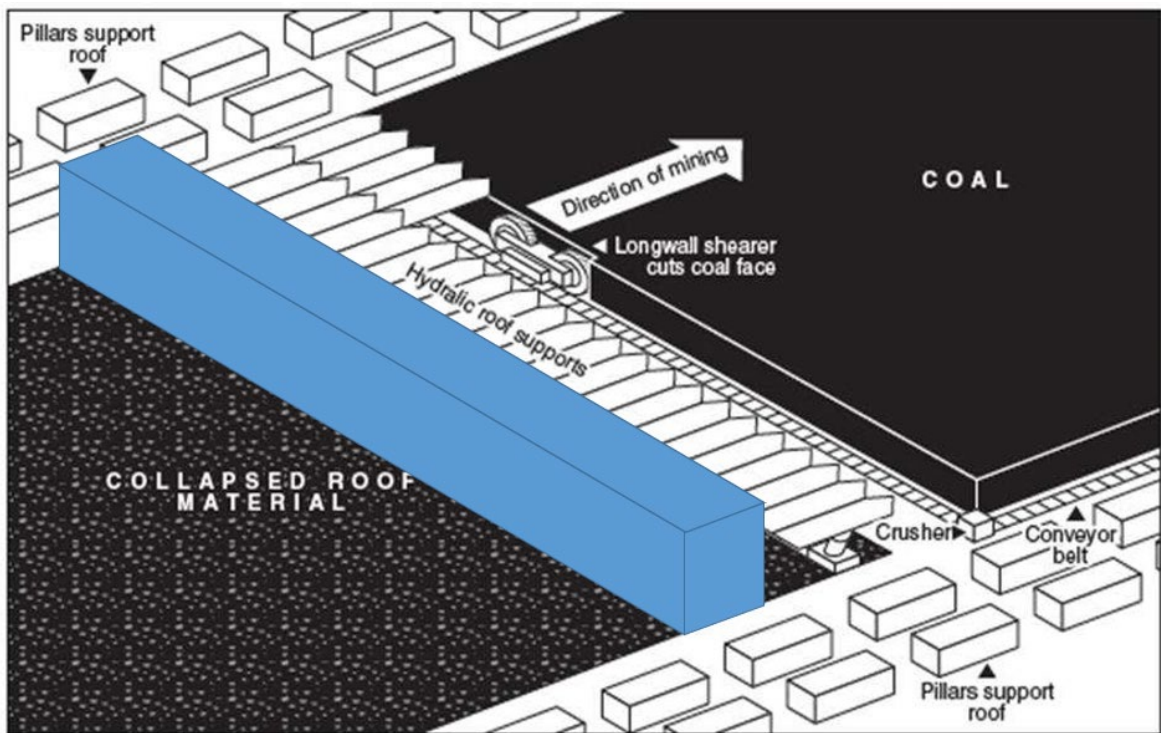
Figure 2.2: Location of roof beam above the gob area in longwall mining

3.1 Beam Theory

In beam theory, a continuous member is broken into thin slices and the shear and moment at each slice is calculated. In some cases, the results at each point can be combined into continuous equations so the behavior at each point can be calculated from a single equation. In the case of sandstone beams over longwall panel roofs, it is assumed that there is a uniform distributed force along the top of the beam and the beam is continuous and uniform. As such, beam theory can be used to approximate the deflection and strain energy along the length of the beam.

3.1.1 Beam dimensions

A beam is defined by three dimensions: length, height, and width, shown in Figure 3.1. Length refers to the horizontal length in the x-dimension and is the largest dimension of the beam. Height is the vertical distance in the y-dimension and is relatively small in comparison to the length. Width refers to the thickness of the beam in the third dimension, and will not be displayed on two-dimensional graphics, but is still a factor in the calculations.
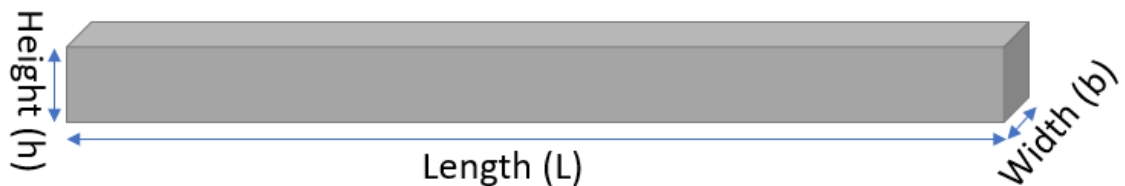
Figure 3.1: Length, width, and height definitions for beams (Length is abbreviated as L, height as h, and width as b.)

3.1.2 Beam calculations

To determine the deflection of the longwall roof, the behavior of the beam formed is needed. In fracturing, the roof will undergo various stages of beam behavior.

3.1.2.1 Built-in

In the process of fracturing, a longwall panel roof will exhibit behavior of various beams. At the first stage of fracture, a longwall roof will most closely resemble the behavior

of a built-in beam, shown in Figure 3.2. At this stage, there are vertical support forces and moments resisting movement on either end, as well as a distributed force along the top of the beam, representing the weight of the overburden on the beam.
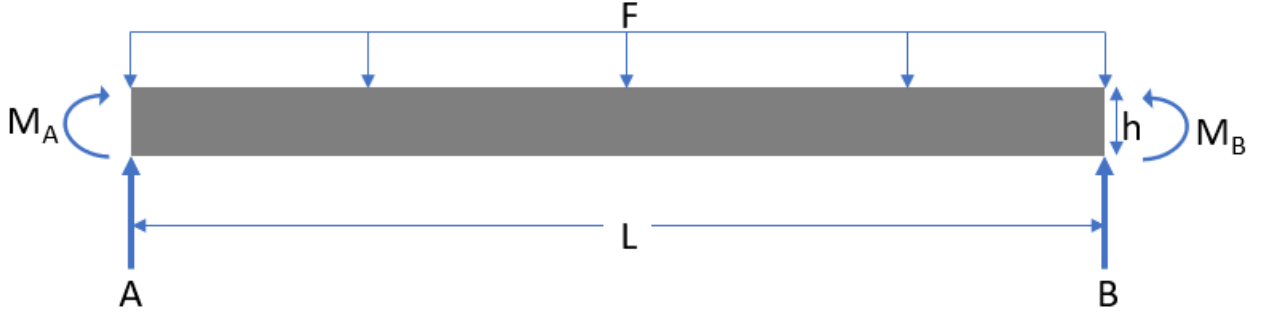
Figure 3.2: Forces and moments on built-in beam

The vertical deflection w_N of the beam a distance x from the end as a result of its weight is calculated using equation 3.1 below (Beer et al., 2015).

$$w_N(x) = \frac{\gamma(1-v^2)}{2Eh^2}(x^4 - 2Lx^3 + L^2x^2) \qquad 3.1$$

Where w_N is the normal deflection of the beam in m at x meters along the length, L, of the beam, γ is the specific weight in MN/m³, v is Poisson's ratio, E is Young's modulus in MPa, and h is the height in m.

3.1.2.2 Simply supported

The next stage of deformation of a longwall panel roof is like that of a simply supported beam. This represents the behavior of fractured roof strata following end fracture of previously built-in beams. In this case, there are no longer moments on the ends resisting movement, and there are only vertical and horizontal support forces and the distributed force along the top, shown in Figure 3.3. As such, the ends are free to rotate about the vertical supports.
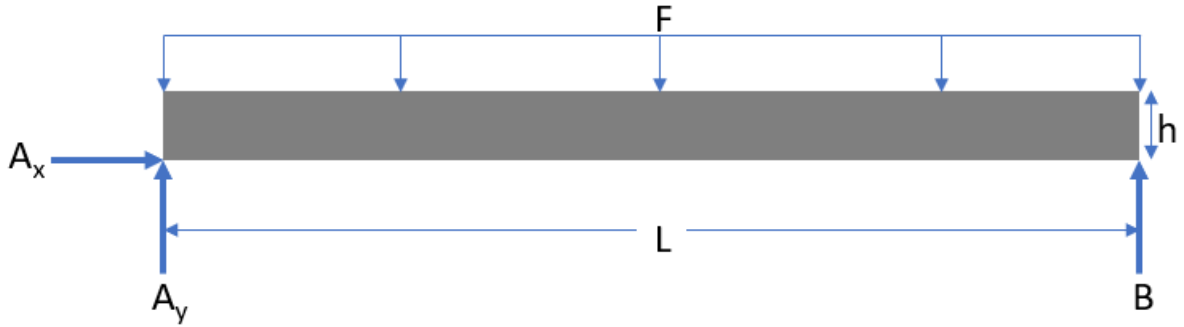
Figure 3.3: Forces on simply supported beam

The deflection along the length of the beam for a simply supported beam is shown in equation 3.2 (Beer et al., 2015).

$$w_N(x) = \frac{\gamma(1 - v^2)}{2Eh^2}(x^4 - 2Lx^3 + L^3x) \qquad 3.2$$

3.1.2.3 Cantilever

Finally, longwall panel roofs will behave most like a cantilever beam, when one end has fractured. Cantilever beams represent the behavior of partially fractured strata, which follow the caving of a simply supported portion of the roof. In this case, one end is free and the other has a vertical support force and a moment, shown in Figure 3.4. The distributed force along the top is still present, as in the other cases.
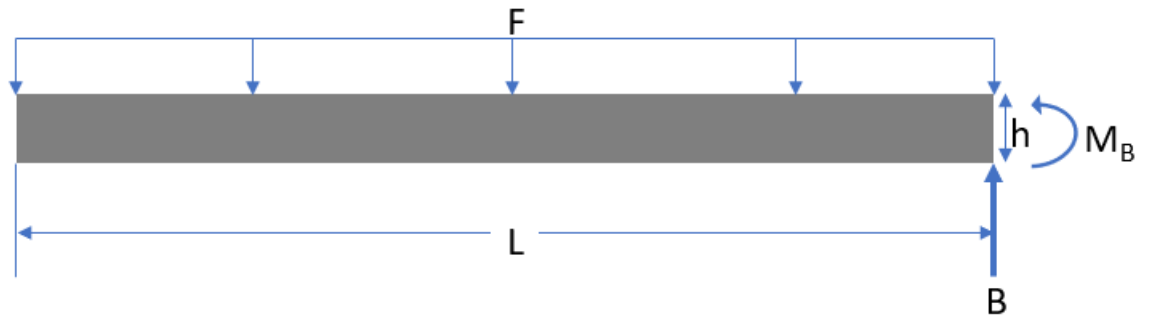
Figure 3.4: Forces and moment on cantilever beam

Equation 3.4 shows the calculation for deflection along the length of a cantilever beam (Beer et al., 2015).

$$w_N(x) = \frac{\gamma(1 - v^2)}{2Eh^2}(x^4 - 4Lx^3x + 3L^4) \qquad 3.3$$

9

Equations 3.1-3.3 are similar, though they differ in their final two terms to account for the difference in deflection for the three cases. The built-in beam cannot rotate on either end, the simply supported beam can rotate but cannot deflect vertically, and the cantilever is completely free on one end and fixed in vertical deflection and rotation on the other.

3.2 Energy

The amount of energy that will be released by a longwall panel roof fracturing will be a combination of strain energy and gravitational energy. The elastic energy stored in a beam due to bending is stored as strain energy. In addition, the potential energy of the suspended weight above an opening is stored as gravitational potential energy. Both the strain energy and gravitational energy are released upon the caving of the strata and are released as seismic energy to the mine workings.

3.2.1 Strain energy

The energy stored due to deflection of the beam is stored as strain energy. The energy is released as seismic energy upon the fracture of the beam and equations for strain energy are dependent on beam theory, similarly to the calculations for deflection.

3.2.1.1 Built-in

In the beginning of strata fracture, the longwall roof is similar to a built-in beam. Equation 3.4 shows the calculation for total strain energy developed in the beam, which is dependent on the geometrical and material properties of the beam (Beer et al., 2015).

$$U_\sigma = \frac{\gamma^2(1-v^2)bL^5}{120Eh} \qquad\qquad 3.4$$

Where U_σ is the strain energy developed in the beam due to bending in MJ, and b is the width in the third dimension in m.

3.2.1.2 Simply supported

The next stage of strata failure is a simply supported beam, where the ends are free to rotate, but both ends still have some support. The equation for strain energy in a simply supported beam is shown in equation 3.5 (Beer et al., 2015).

$$U_\sigma = \frac{\gamma^2(1-v^2)bL^5}{20Eh} \qquad\qquad 3.5$$

3.2.1.3 Cantilever

Finally, the beam exhibits behavior similar to a cantilever beam, and the strain energy equation is shown in equation 3.6 (Beer et al., 2015).

$$U_\sigma = \frac{3\gamma^2(1-v^2)bL^5}{10Eh} \qquad\qquad 3.6$$

Equations 3.4-3.6 are similar, and the only difference exists in the multiplication factor. Cantilever beams have the highest multiplication factor of $\frac{3}{10}$, indicating that they store the most strain energy for the same size beams. This follows logically, as they are the freest to deform and can store the most strain energy. However, they are the most fractured and thus the shortest, so the shorter length results in a lower strain energy developed than the longer simply supported and built-in beams.

3.2.2   Bending plate element

Another method of calculating the strain energy developed in a bending member is to consider the beam a narrow bending plate. Equation 3.7 calculates the strain energy as an integral of the stresses and strains throughout the volume (Logan, 2022).

$$U_\sigma = \frac{1}{2}\int_V \left(\sigma_x\varepsilon_x + \sigma_y\varepsilon_y + \tau_{xy}\gamma_{xy}\right)dV \qquad\qquad 3.7$$

Where σ is the normal stress in the x- and y- directions, ε is the normal strain, τ_{xy} is the shear stress, and γ_{xy} is the shear strain, over a differential volume dV.

3.2.3   Gravitational potential energy

Gravitational potential energy represents the amount of energy that will be released due to the weight of the beam, should it fall a distance u. Because the beam has already deformed, the differential between the opening height left from mining and the distance that the section of beam dropped is the remaining height that the beam can fall, as shown in equation 3.8.

$$u = H - w \qquad\qquad 3.8$$

Where u is the distance the beam will fall, H is the opening height, w is the distance the beam deflected, calculated using equation 3.2.

The total gravitational potential energy is calculated as an integral of the deflections multiplied with the weight of the beam, along the full length of the beam, as shown in equation 3.9 (Serway & Jewett, 2018).

$$P_g = \tilde{m}g \int_{beam\ length} u\ dx \qquad\qquad 3.9$$

The continuous integral is approximately equal to a discrete integral of n pieces along the length of the beam, shown in equation 3.10.

$$P_g = \tilde{m}g \sum_{i=0}^{n} u_i = \gamma hb \sum_{i=0}^{n} u_i \qquad\qquad 3.10$$

Where P_g is the total gravitational potential energy, $\tilde{m}$ is the mass per unit length, g is the acceleration of gravity, and u_i is calculated using equation 3.8. Equation 3.10 is used with the specific weight, height, and width of the sandstone for 1 m sections along the length of the beam to determine the total gravitational potential energy.

The presence of gob beneath the beam reduces the drop height of the beam, reducing the gravitational energy released by the beam. As u_i decreases due to the presence of material below the beam, P_g decreases.

3.3   Seismic Magnitude

When the longwall roof beam caves, the strain and gravitational energy stored in the beam is released to the surrounding mine workings in the form of seismic energy. Gutenberg (1945) calculates the seismic magnitude of an energy release using equation 3.11, shown below.

$$\log_{10} E = 1.5M_S + 11.8 \qquad\qquad 3.11$$

where E is the energy in ergs, and M_S is the magnitude of the seismic event. 1 erg is 10^7 Joules. There are several methods for calculating seismic magnitude. Díaz-Mora and González-Fallas (2022) and Okal (2019) use the same seismic magnitude equation shown

above. The applicable range for this equation is not strictly provided, but it is necessary that the size of the seismic event be relatively small in comparison to the area being monitored for the equation to be applicable (Panza et al., 2014). Hayes and Wald use a two-step calculation using equations 3.12 and 3.13. This method results in similar values to equation 3.11.

$$Moment(M_0) = rigidity \times area \times slip \qquad 3.12$$

$$Moment\ magnitude(M_W) = \frac{2}{3}\log_{10}(M_0) - 10.7 \qquad 3.13$$

Using equation 3.11 in combination with strain energy calculated with equation 3.5 and gravitational potential energy calculated with equation 3.10, the seismic energy released as a result of strata caving in a longwall operation is calculated analytically. The Richter scale is used for this analysis, as the seismic emissions are relatively small-scale compared to earthquakes and local to the mining operation.

Following the analytical approach, a series of numerical models are developed using the two-dimensional modelling software, RS2, to approximate the strain energy and gravitational energy developed in the longwall panel roof beam ("RS2," 2021). The numerical models are used to model the stresses, strains, and deflections of the panel roof beams to then calculate the energy that will be released when the strata caves. The determination of stresses and strains along the beam allow for better calculation of the energy stored in the beam, that will then be released upon beam failure. If only deflections and strain energy were needed, the analytical calculations would suffice. Numerical modelling provides the stress and strain stored in the beam to improve the energy calculation. The results of the numerical models are compared to the analytical approach to verify the models. By using numerical models, a wide variety of parameters could be adjusted to determine their effect on the energy developed in the roof beam.

4.1 Model selection

A variety of models are developed to determine a sufficient base model that could be compared against to model various parameters. For a beam to form over a longwall panel, the roof material must be competent, so strong sandstone is used for the roof beam models. The headgate and tailgate system are simplified into 50 m long solid coal pillars on either end of the beam. The overburden force on the top of the beam is ignored. It is assumed there is bed separation between the beam and the overlying strata, and the overburden weight does not affect the beam.

4.1.1 Beam length

The first tests were done to determine the length of the roof panel to be used in calculations. The unsupported length of the beam is 330 m while entire panel width including the headgate and tailgate systems is 430 m. Figure 4.1 shows a comparison of the deflection along the length of the beam results from various numerical models and analytical calculations. The numerical models exhibit a variety of end behaviors. Model A has no end supports on the two ends of the roof beam, model B has rollers on the ends of the beam to simulate a fixed end, model C is the same as A, but has a reduced coal pillar

height, and model D is the same as A but has a joint modeled between the beam and the coal pillars supporting either end. The analytical equations are calculated using equation 3.2 for built-in beams and equation 3.3 for the simply supported beams. For the analytical equations, 330 m and 430 m beams are compared to the deformation over the entire width of the model.
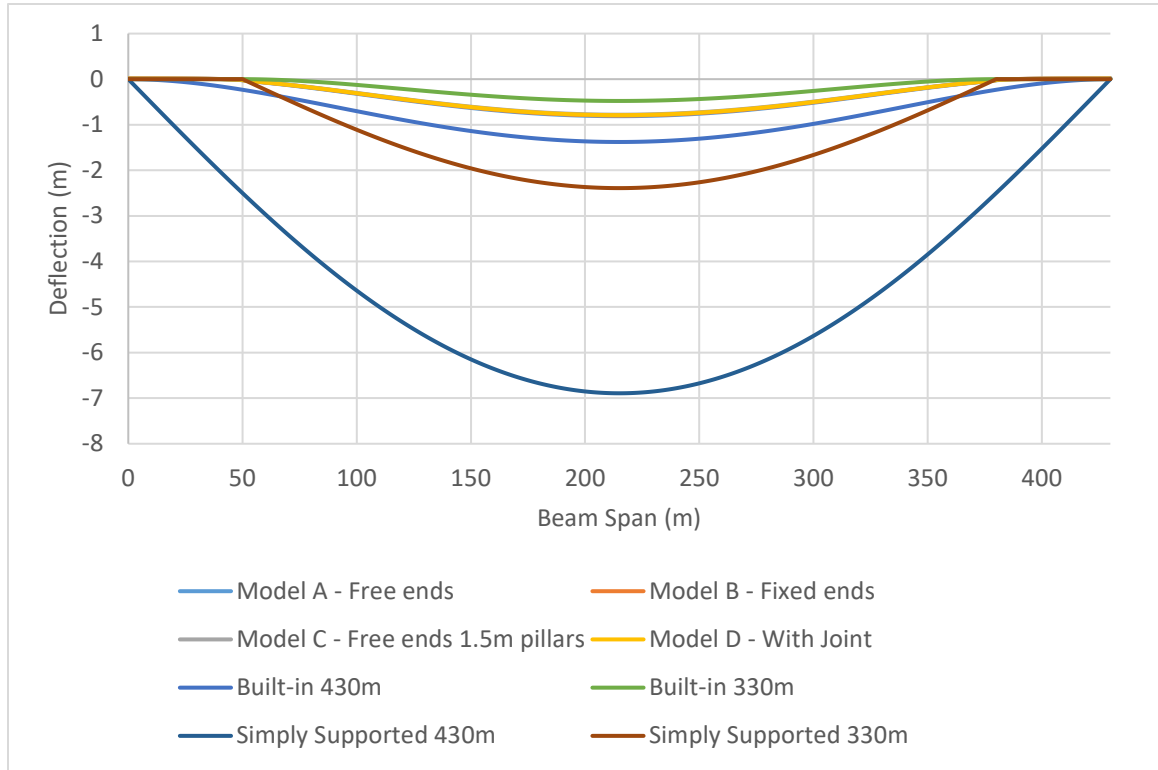
Figure 4.1: Numerical and analytical models for 330 m and 430 m length beams

As can be seen in Figure 4.1, the numerical models fall between the analytical results of the 330 m beams. The deformation of the 430 m calculations significantly exceeds the numerical models at all points. As such, a 330 m beam is used in all models and calculations going forward. The pillars on either end of the model act as rigid supports, limiting deflection of the beam at the ends.

Numerical models represent a plane strain model, representing a unit thickness of an infinite plate. As such, the stresses in all three dimensions are considered, while the strain in the longitudinal direction is zero. Therefore, the numerical models differ from the analytical equations, which represent thin beams.

15

4.1.2   Comparison to analytical equations

Next, the deflection results of the models and equations are compared more thoroughly. The difference in the boundary conditions of the RS2 models are described in Section 4.1.1. Figure 4.2 shows a comparison of the modeled and calculated deflections along the length of the roof beam. All four of the models appear to overlap and the deflections are between those calculated for the built-in and simply supported beams (equations 3.2 and 3.3, respectively). This indicates that the behavior of a longwall roof beam is between that of a built-in beam and a simply supported beam. The ends of the beam are able to rotate more than the completely fixed built-in beam but are not as entirely free to rotate as the simply supported beam.
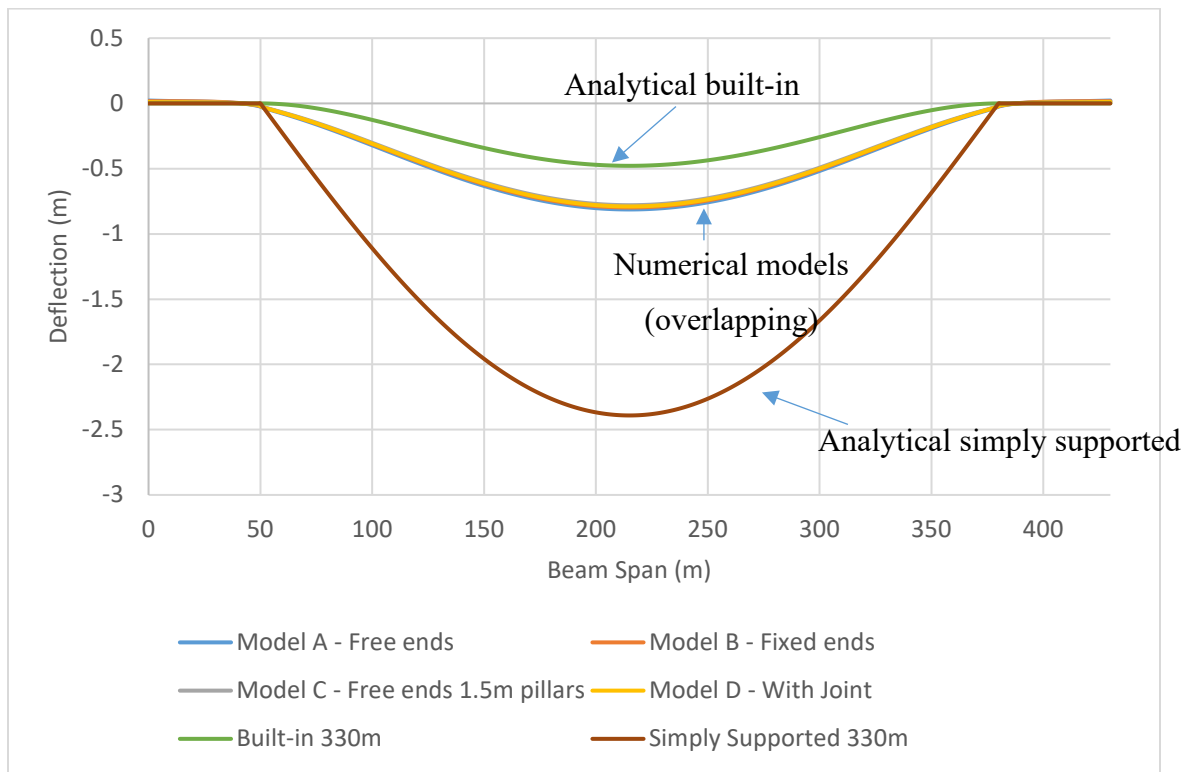
Figure 4.2: Comparison of analytical and numerical models of 330 m beam deflections

A key difference between the analytical equations and the numerical models is that the numerical models represent a slice of an infinitely long plate, resulting in the models being in plane strain. Stresses in all three dimensions are considered, but strain in the third dimension is zero. The equations, on the other hand, do not take into account external stress

or strain, and only consider the beam properties. The equations model a two-dimensional beam, rather than a slice of an infinite plate, and thus differ from the numerical models.

Following this analysis, the numerical models are shown to closer represent the behavior of an actual roof beam in comparison to the analytical approach, and will the main tool used in the analyses.

4.1.3 Beam end restraints

The effect of restraining and freeing the ends of the sandstone beam are compared, as shown in Figure 4.3. There is a slight difference in the four models' deflections, but the results largely overlap. Model A shows a somewhat higher deflection than the remaining models, with 3 m high coal pillars and sandstone beam ends not constrained. Model C has slightly less deflection than the other models, with 1.5 m coal pillars and free ends. Models B and D are between these values, demonstrating that the use of free versus fixed ends does not greatly affect the deflection, nor does using a joint between the sandstone and coal pillars.
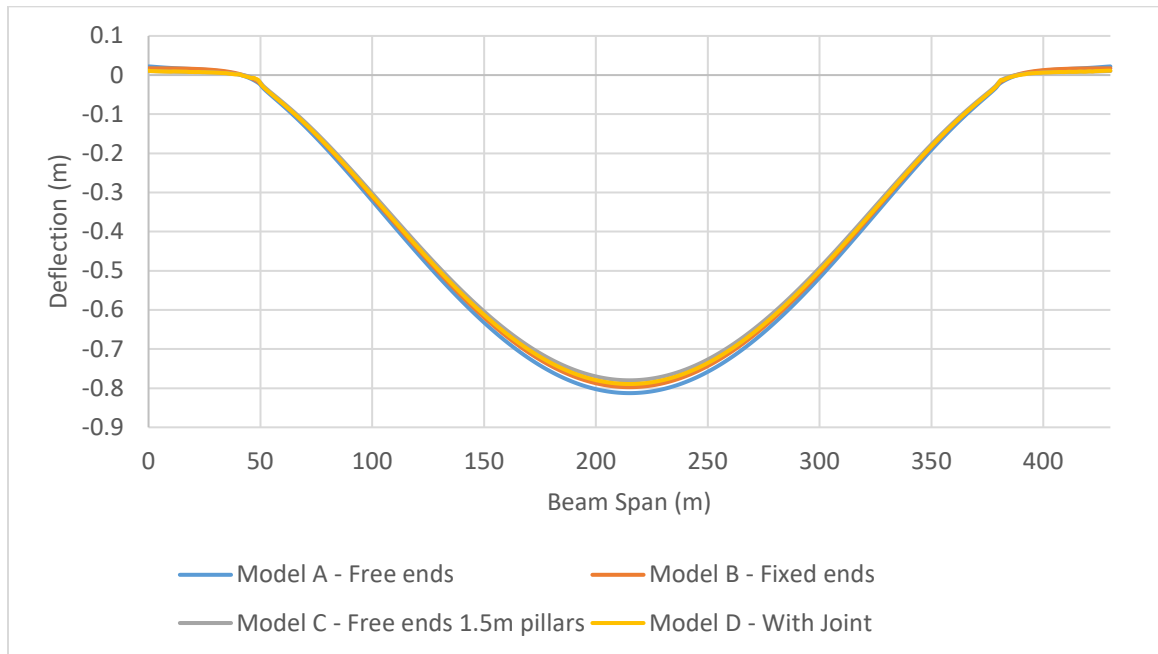
Figure 4.3: Comparison of RS2 model end restraints

Model C is used as the base model of the following analyses as the lack of end restraints decreases trial run time slightly and the total coal pillar height is twice the

modeled height, so the 1.5 m pillars used represent 3 m high pillars, a more realistic height than the 6 m high pillars in the other models.

4.1.4   Effect of elastic deformation of pillar system

An elastic model creating a full mesh of the entire overburden is created to determine the effect of elastic deformation of the pillar system on the beam bending. The full beam deflection results are shown in Figure 4.4.
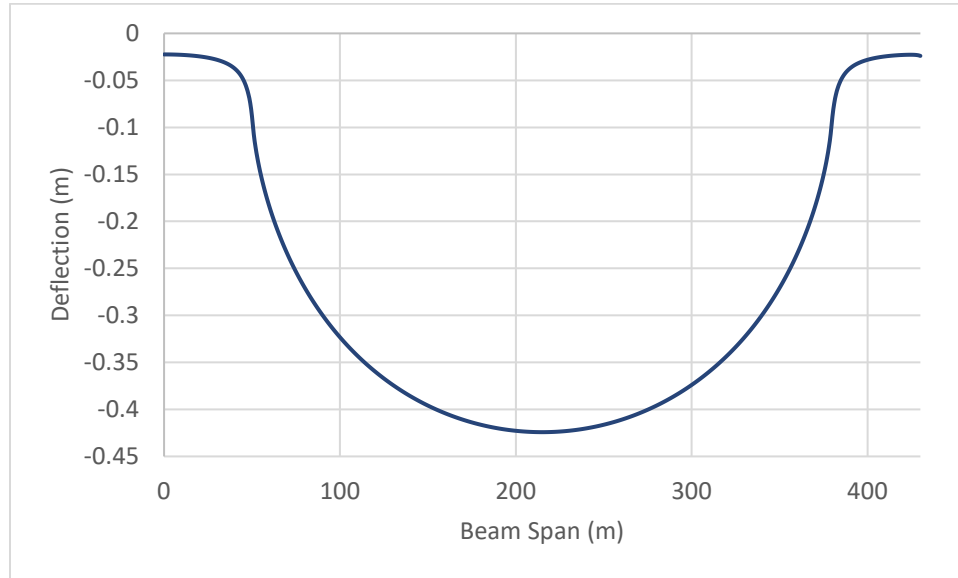
Figure 4.4: Beam deflection with elastic pillar deformation modelling full overburden

The shape of the beam deflection differs from the previous models, as the beam compresses the pillar at the corner. This model resulted in excess deformation at the edge of the pillars, that does not match the previous analysis. Furthermore, the model compressed the coal pillars, resulting in a nonzero deflection over the pillars.

Depth in the models analyzed is instead entered using the RS2 form shown in Figure 4.5.
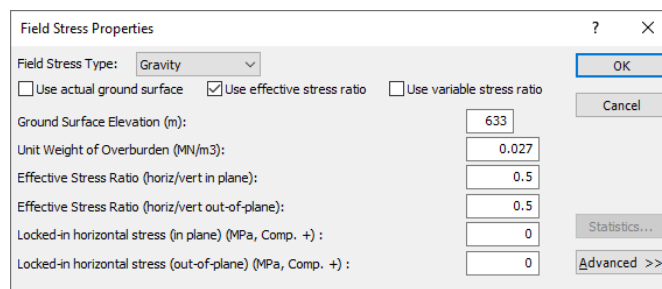
Figure 4.5: RS2 field stress properties menu

18

4.1.5 Depth

An analysis of the effect of depth on the model and equations shown in Figure 4.6, modelling a full mesh of the overburden, as in Figure 4.4. Increased depth is shown to increase the maximum deflection, though does not have a great effect. The deflection is also exaggerated as the deflection of the pillars is increased with increased depth, while the pillars would already be compressed and would not greatly compress further. Modelling in RS2 while changing depth using the form shown in Figure 4.5 does not affect deflection, and the analytical equations do not consider external load.
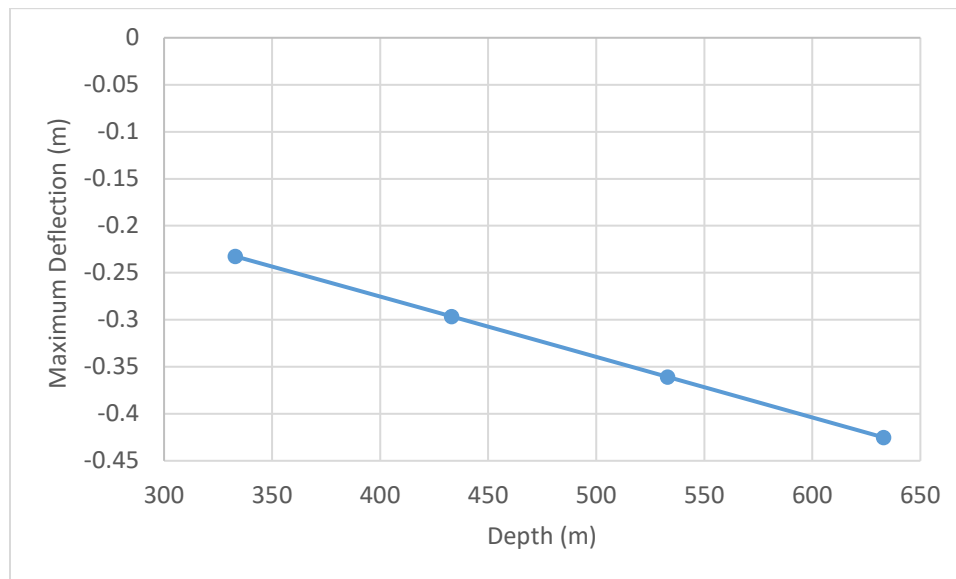
Figure 4.6: Maximum deflection in beam at varying depths of cover

4.1.6 Horizontal to vertical stress ratio

The impact of horizontal to vertical stress ratio on energy is observed in Figure 4.7. Deflection increases slightly with increased horizontal stress, as the stresses and strains increase, but does not significantly affect the deflection results. As shown in Figure 4.2, the simply supported analytical results have much greater deflection at the center, and the built-in beam has less deflection, accounting for the variation in deflection from the RS2 model. The horizontal to vertical stress ratio is also modelled for the full overburden mesh (not shown) and also does not affect deflection.
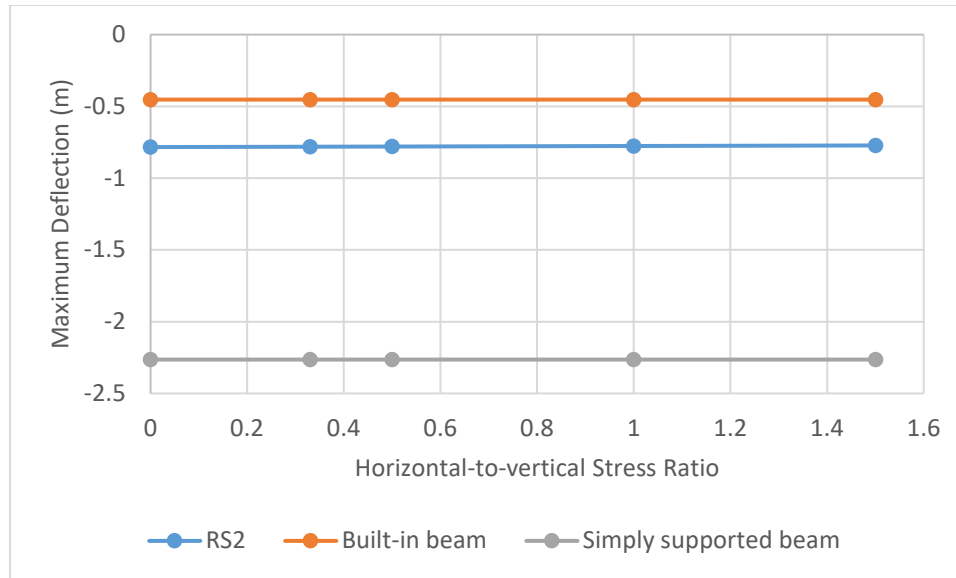
Figure 4.7: Maximum deflection at varying horizontal-to-vertical stress ratios

4.2 Model Parameters

The models are created using RS2, a two-dimensional modelling software. RS2 performs calculations in plane strain, which assumes that there is no strain in the third dimension. Because of this, the models created are unit width taken out of an infinitely long plate so strains in the third dimension are negligible, but stresses in the third dimension are nonzero. The models are also done assuming that the materials are isotropic, homogeneous, and elastic.

4.2.1 Model assumptions

Assumptions are made for the beam in order to allow the complex phenomenon to be represented with a two-dimensional model. It is assumed that the material is isotropic, homogeneous, and elastic. External load due to overburden is assumed to be zero, as there is assumed to be bed separation between the beam and the overlying strata. The model is created in plane strain, so the strains in the third dimension are assumed to be zero. Stresses in all three dimensions are nonzero. Plane strain is used as it assumes the model extends infinitely in the third dimension, and a slice of a long plate is modeled. As longwall panels are much longer than they are wide, this assumption is valid.

4.2.2 Elastic model properties

Esterhuizen et al. (2010) provides standards to use when using numerical modelling with coal and surrounding strata. Table 4.1 and Table 4.2 display the material properties used in the numerical models for sandstone and coal, respectively.

Table 4.1: Sandstone elastic properties (Esterhuizen et al., 2010)

Unit weight (kN/m^3)	24
Poisson's ratio	0.25
Young's modulus (MPa)	20,460
Hydraulic properties	Drained
Initial element loading	Field stress and body force

Table 4.2: Coal elastic properties (Esterhuizen et al., 2010)

Unit weight (kN/m^3)	19.6
Poisson's ratio	0.25
Young's modulus (MPa)	3,000
Hydraulic properties	Drained
Initial element loading	Field stress and body force

Both the sandstone and coal are loaded under field stress and body force. The external load due to overburden is assumed to be zero, as it is assumed that the beam separates from the overlying strata and the overburden is not applying additional weight to the beam.

RS2 creates a mesh in the modelled components so that each element in the mesh can move and the relations between neighboring mesh elements reflect the material properties inputted. For these models, the mesh properties used are shown in Table 4.3.

Table 4.3: Mesh properties

Mesh setup	Uniform
Element type	6-node triangles
Number of mesh elements	~10,000

4.2.3   Support geometry

The boundary conditions for the model are used to restrain the model to realistic deformation. The model cannot be over- or under-restrained, or a numerical solution cannot be determined. The models are restrained in the x- and y-directions using a pin at the lower left-hand corner of the model and are restrained along the bottom of the model in the y-direction using rollers, shown in Figure 4.8.
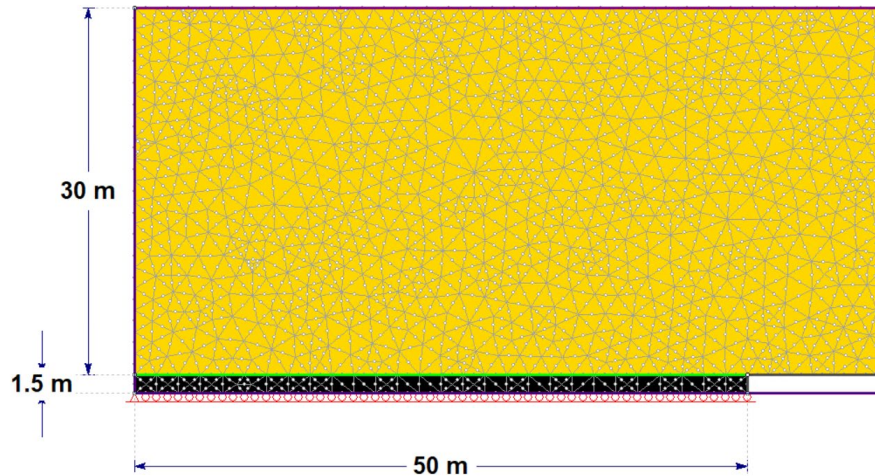

Figure 4.8: Beam support geometry

The external supports of the sandstone beam are shown to have minimal effect on the deflection of the roof beam, as shown in Figure 4.3, and are left free in the models. In doing so, the models assume that the sandstone beams have fractured from the neighboring beams on either end. The left-hand end of the model is displayed in Figure 4.8, showing the lack of end restraints on the yellow sandstone beam.

Restraining along the bottom of the model results in the restraints being along the bottom of the modelled coal pillar, shown in black in Figure 4.8. The use of restraints indicates a reflection across the axis being restrained. Because of this, the coal pillar is assumed to be reflected across the x-axis, and the modelling of a 1.5 m coal pillar is indicative of a real pillar height of twice the modelled height, or 3 m.

The overall design of the model is shown in Figure 4.9. Figure 4.10 displays the vertical deflection results of the base model with displacement vectors.

Figure 4.11 and Figure 4.12 show the stress results with and without stress trajectories. Figure 4.13 shows a close-up of the stresses around the coal pillar, and Figure 4.14 shows the strain results.
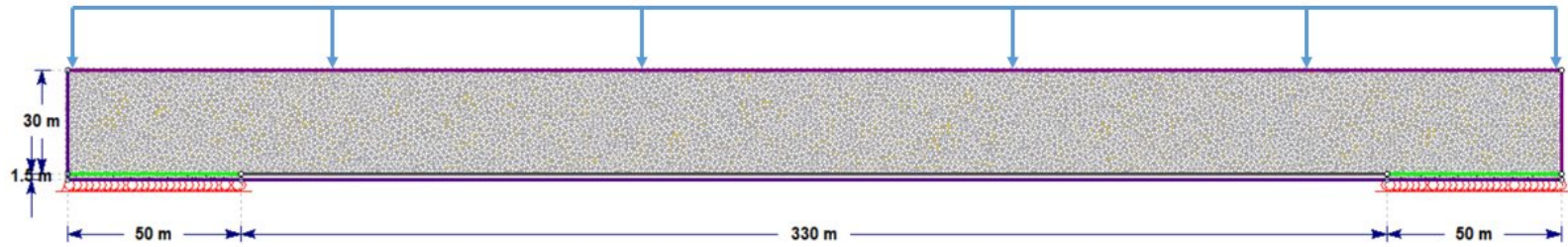
Figure 4.9: RS2 model dimensions and supports
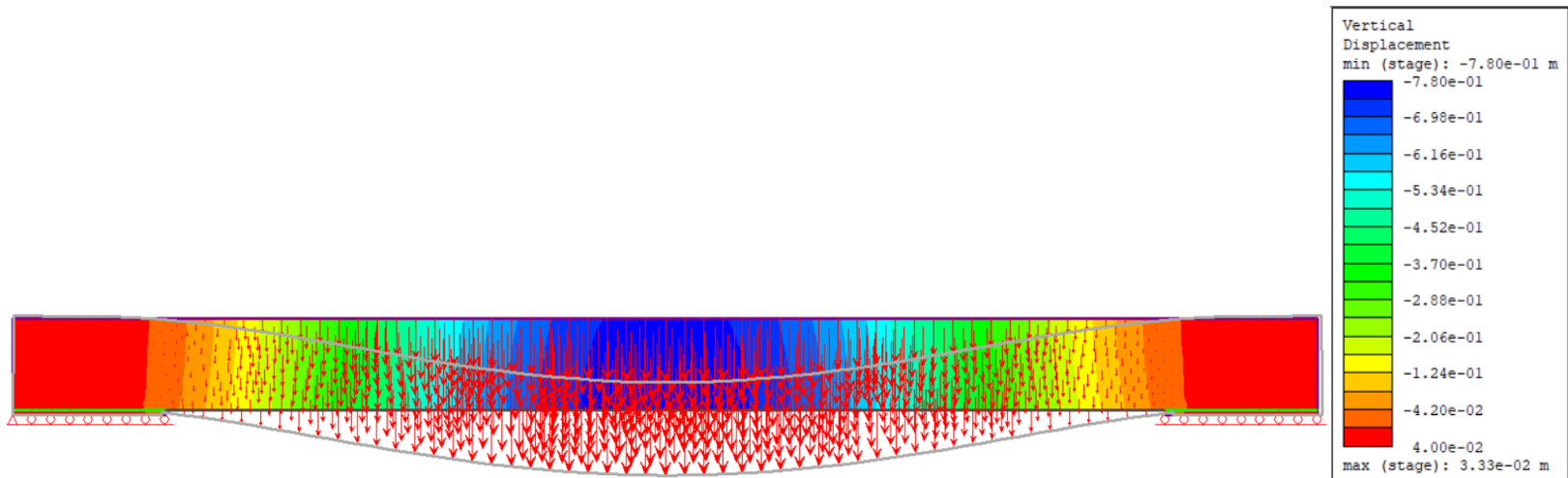
Figure 4.10: RS2 model vertical deflection results
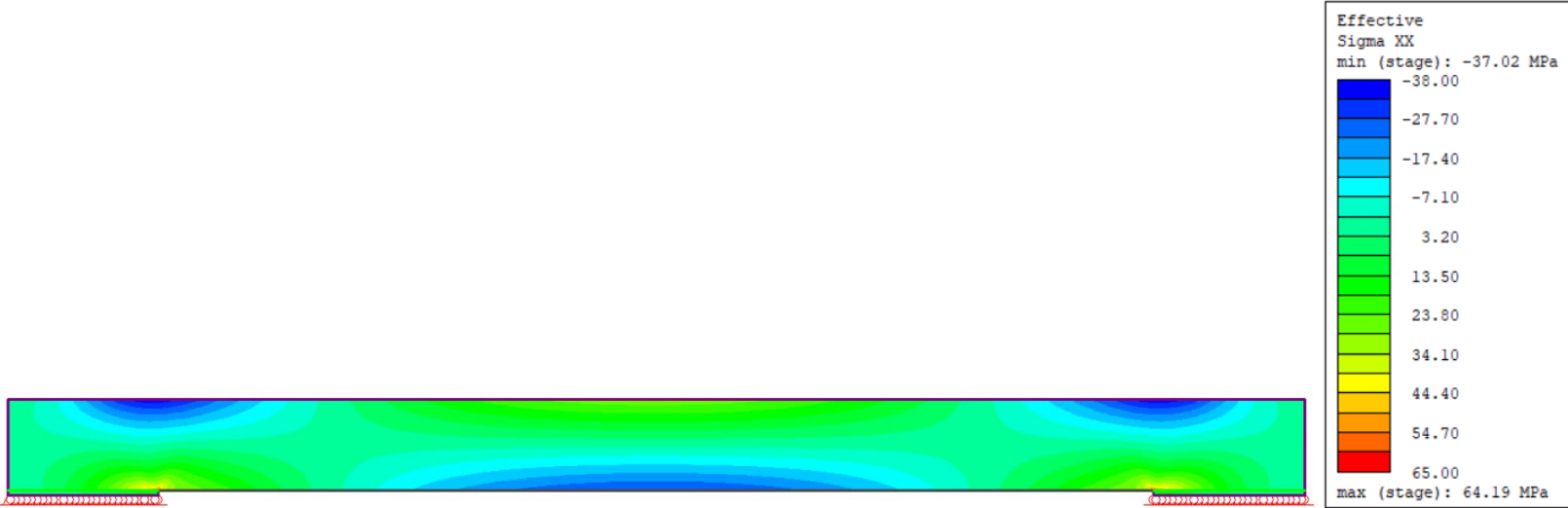
Figure 4.11: Stress results
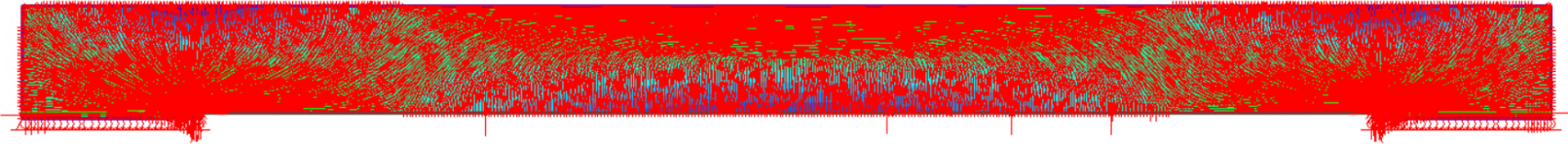
Figure 4.12: Stress with stress trajectories results
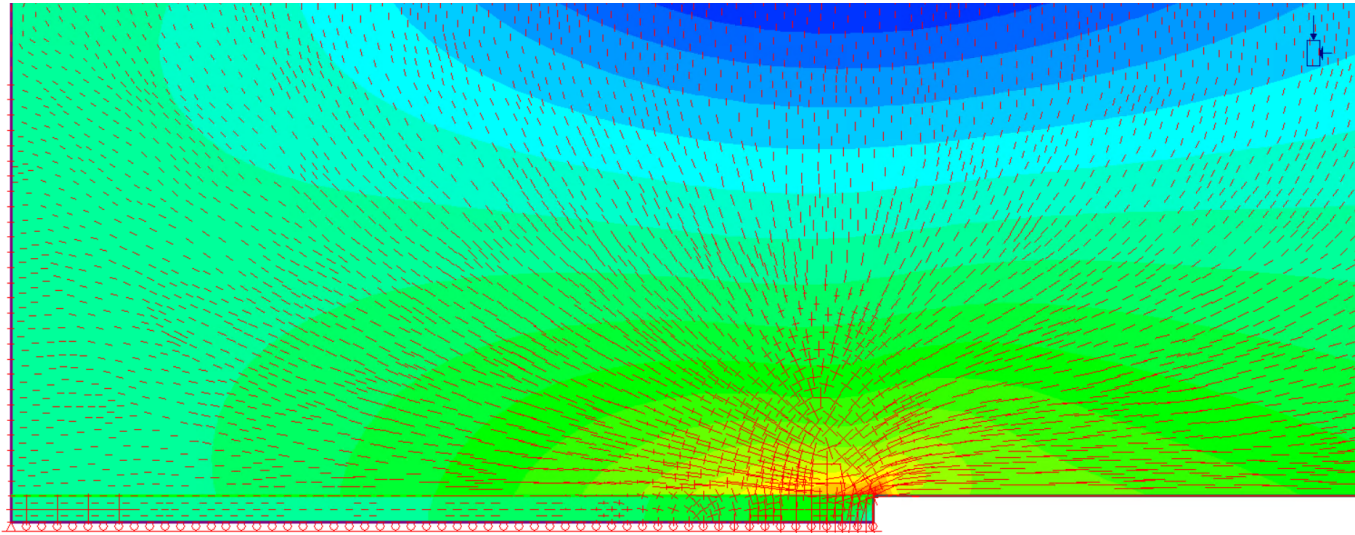
Figure 4.13: Stress around pillar with stress trajectories


```
Strain XX
min (stage): -6.45e-03
        -6.50e-03
        -6.06e-03
        -5.62e-03
        -5.18e-03
        -4.74e-03
        -4.30e-03
        -3.86e-03
        -3.42e-03
        -2.98e-03
        -2.54e-03
        -2.10e-03
        -1.66e-03
        -1.22e-03
        -7.80e-04
        -3.40e-04
         1.00e-04
         5.40e-04
         9.80e-04
         1.42e-03
         1.86e-03
         2.30e-03
max (stage): 2.30e-03
```
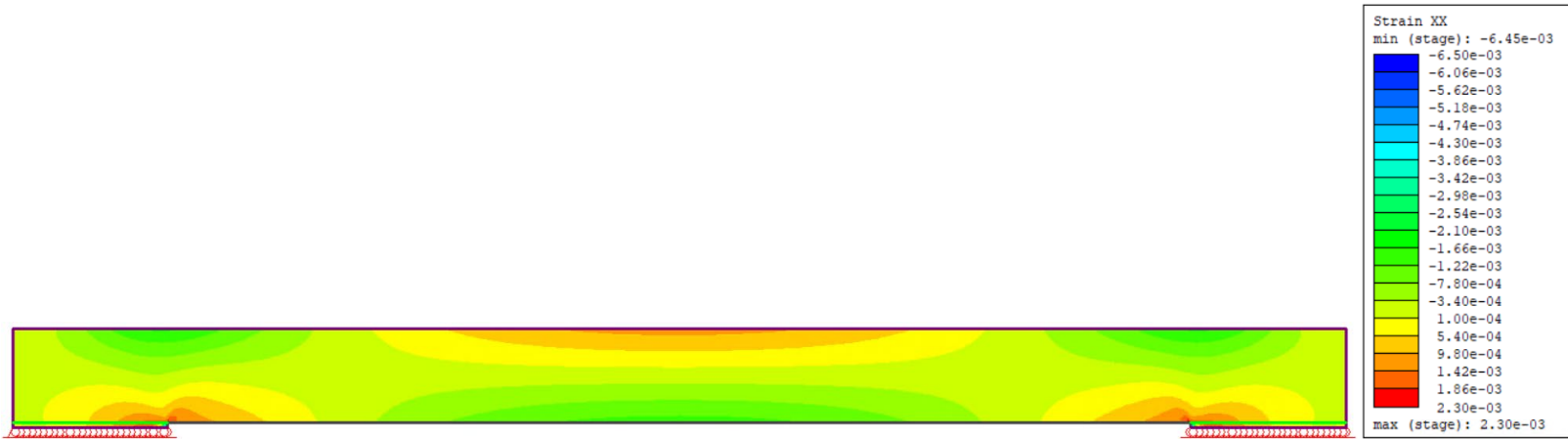
Figure 4.14: Strain results

4.3   Parametric Analyses

Several parametric analyses are conducted to ensure the models follow predicted behaviors.

4.3.1   Elastic modulus

Young's modulus is varied from 10,000-40,000 MPa, at increments of 2,500 MPa to observe the behavior of the models. Beam height is 30 m, width is 1 m, and unsupported length is 330 m. Figure 4.15 displays the deflection results of this analysis. As the elastic modulus increases, the maximum deflection of the beam decreases.
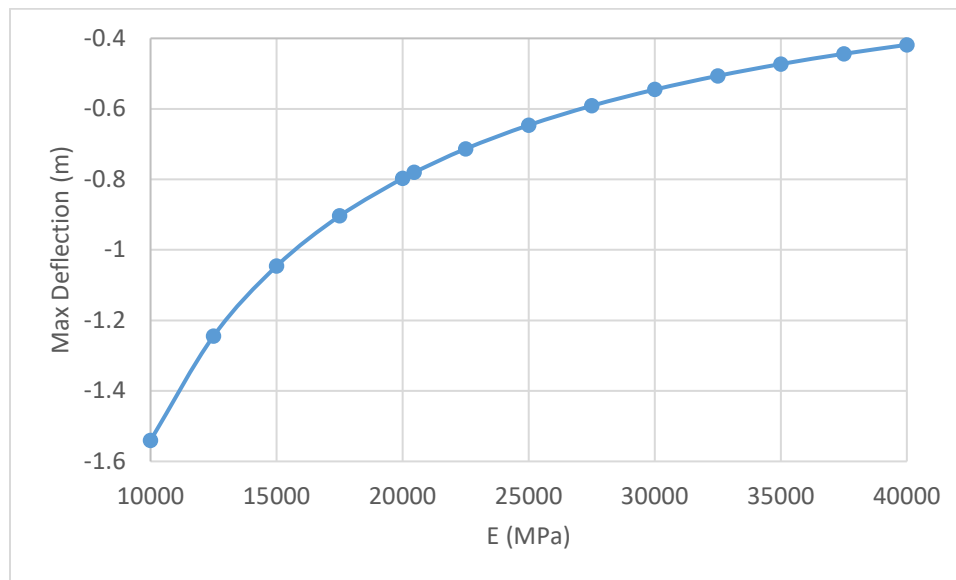
Figure 4.15: Parametric analysis of maximum beam deflection at various elastic moduli

An increase in Young's modulus indicates an increase in the stiffness of the beam. A stiffer beam is expected to deform less than a more flexible beam under the same loading conditions. The results of the graph reflect this behavior, as expected.

4.3.2   Beam height

Beam heigh is varied from 10-100 m, at increments of 5 m to observe the model's behavior. Beam width is 1 m, and unsupported length is 330 m. Figure 4.16 displays the maximum deflection results of this analysis. As beam height increases, deflection decreases, seeming to approach a limit of 0 deflection.

Figure 4.16: Parametric analysis of maximum beam deflection at various beam heights

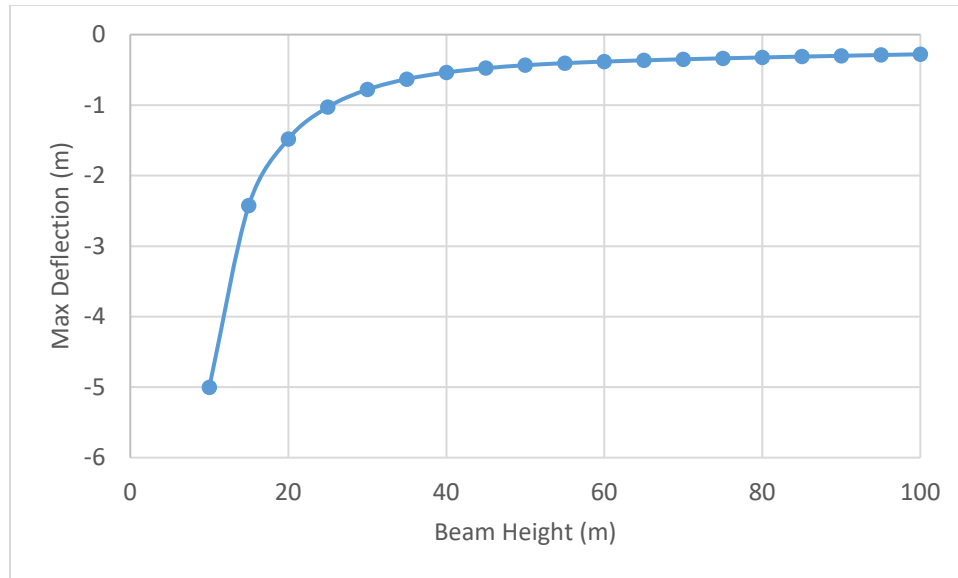An increase in beam height increases the stiffness of the beam, and a stiffer beam is expected to deform less than a more flexible one under the same loading conditions. This behavior is exhibited by the model, as expected.

The seismic energy that will be released by the sudden caving of a stiff longwall roof beam is determined by the results of the analytical and numerical approaches.

5.1 Comparison of Analytical Calculations and Models

The models have been verified in terms of deflection, as demonstrated in Section 4.1.2: Comparison to analytical equations. The energy calculations are approximations for longwall roof bending and failure for gravitational potential energy and strain energy.

5.1.1 Strain energy

The x-, y- and shear stress and strain values taken at 1 m intervals along the bottom of the RS2 model beam are used in equation 3.7 for a 1 m wide beam to calculate the strain energy of the entire beam. Beam height is 30 m, and unsupported length is 330 m. This is compared to the analytical approach for strain energy, calculated using equation 3.5. The parametric analysis conducted in Figure 4.15 is repeated for a strain energy analysis. The results of a series of models at different elastic moduli are shown in Figure 5.1.
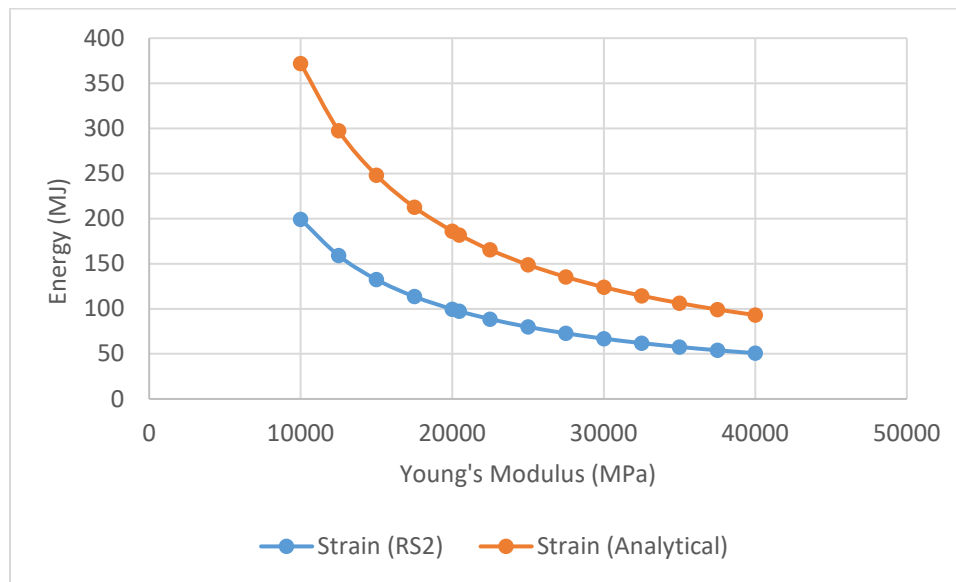

Figure 5.1: Parametric analysis of strain energy and elastic modulus

Both curves follow a decreasing, negative slope, indicating that as the stiffness of the beam increases, the strain energy decreases, reaching a potential limit of 0. As the beam increases in stiffness, it does not deflect as much, and stores less energy due to strain. The

28

apparent limit of 0 indicates that the beam approaches a point where it will not deflect at all for a conceptual value of infinite stiffness. The strain energy calculated using the analytical approach is greater than that using RS2. As the simply supported model is used for the analytical approach, and the simply supported equation yielded three times the deflections than the RS2 model, it follows that the analytical approach yields twice the value of energy than RS2.

The analysis was repeated using models at varying beam heights, as in the analysis shown in Figure 4.16, and is shown in Figure 5.2. Beam height is 30 m, width is 1 m, and unsupported length is 330 m.
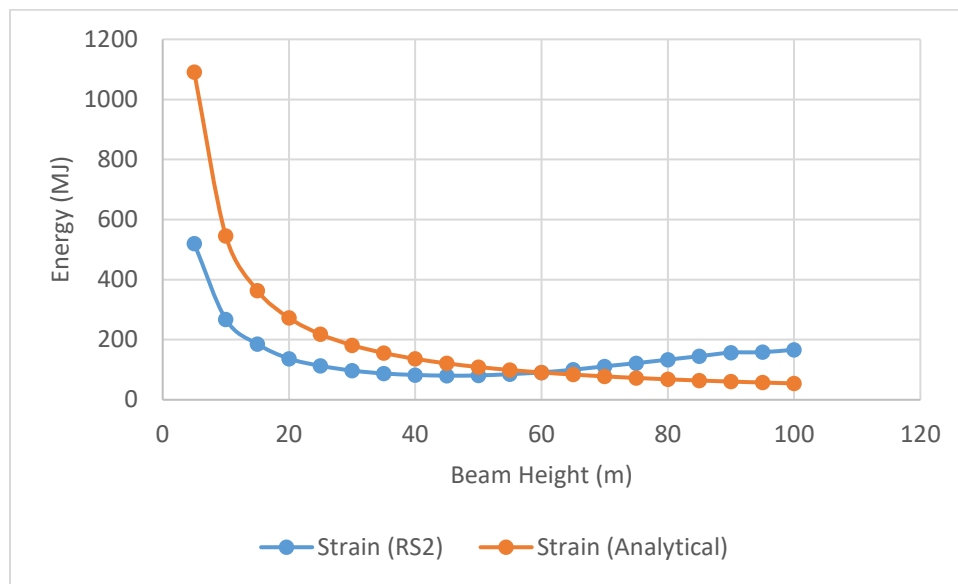
Figure 5.2: Parametric analysis of strain energy and beam height

Similarly, to the elastic modulus analysis, the energy curves decrease as beam height increases, and level off. This indicates that with increased beam height, the beam increases in stiffness and deflects less, storing less strain energy. Around 60 m, the strain energy calculated in RS2 appears to increase above the values of the analytical analysis. At that point, the size of the model began to exceed the granularity of the nodes. The mesh was too coarse to capture all of the data with an increased area to model, and the energy calculations were not as accurate as they are for the thinner beams.

5.1.2 Gravitational energy

The gravitational energy calculated using the deflections of the beam determined using the numerical model at 1 m intervals for a 1m wide beam and equation 3.10 is compared with the gravitational energy determined using the deflections calculated with equation 3.2 and energy calculated using equation 3.10. Beam height is 30 m, width is 1 m, unsupported length is 330 m, and drop height is 3m. The results of the analysis for varying elastic moduli, similar to the analysis done in Figure 4.15, are shown in Figure 5.3.
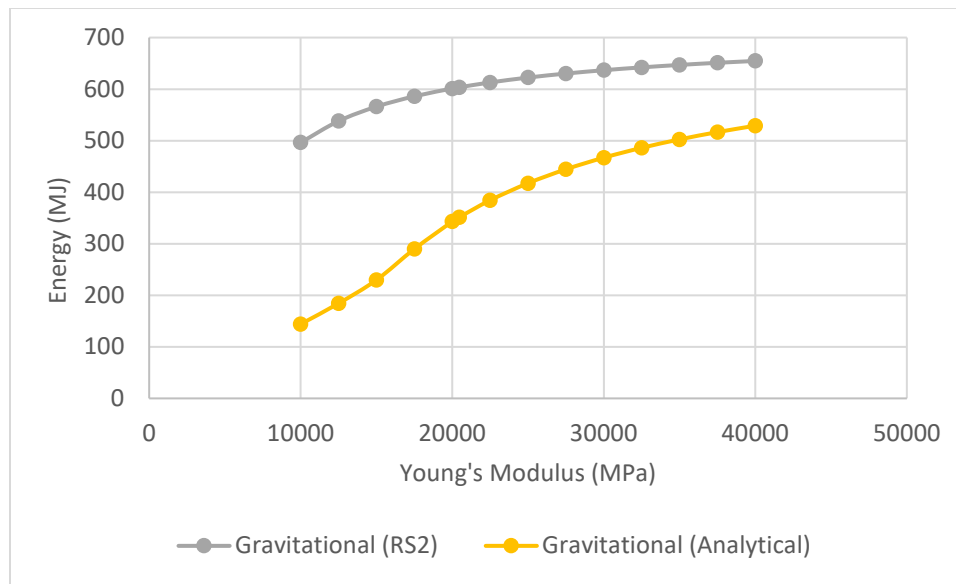
Figure 5.3: Parametric analysis of gravitational potential energy and elastic modulus

As Young's modulus increases, the gravitational potential energy is shown to increase. The decrease in deflection of stiffer beams under the same loading conditions allows the beam to have a higher distance left to potentially fall. Thus, it follows that the increase in elastic modulus results in increasing gravitational energy. Furthermore, the analytical approach was done using the simply supported beam, which had higher deflection than the numerical model, so the beam has less distance to fall and less gravitational energy. The presence of gob below the beam will dissipate energy, so the energy released to the mine will be less than the values calculated. Furthermore, the material will swell upon fracturing, reducing the height that it will fall and further reducing the gravitational energy released.

The analysis is repeated with varied beam heights, like the analysis shown in Figure 4.16, is shown in Figure 5.4. Beam height is 30 m, width is 1 m, unsupported length is 330 m, and drop height is 3m.
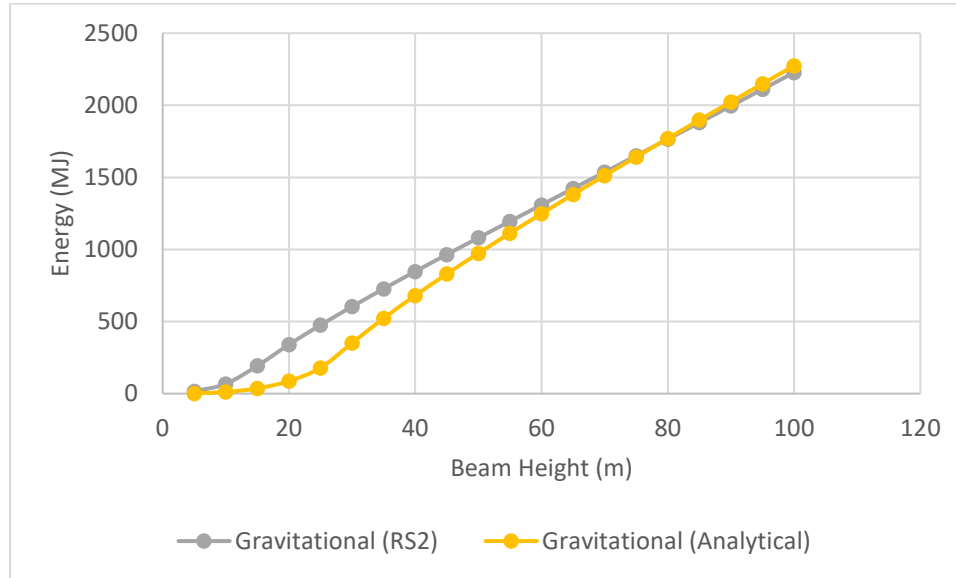

Figure 5.4: Parametric analysis of gravitational potential energy and beam height

In this analysis, the gravitational potential energy sharply increases with increasing beam height. The increase in weight resulting from the increase in beam volume as height increases allows for a greater release of energy when the beam falls. The analytical and RS2 models follow very similar curves, indicating that the increase in the weight, affecting both calculations equally, is the driving factor.

5.1.3 Relative magnitudes of gravitational and strain energy

The energy that has the greatest impact on the seismic energy released is the energy with the greatest magnitude. Figure 5.5 illustrates the relative magnitudes of strain and gravitational energy for varying Young's moduli, and Figure 5.6 shows their relative magnitudes for varying beam heights. Beam width is 1 m, unsupported length is 330 m, and drop height is 3m.
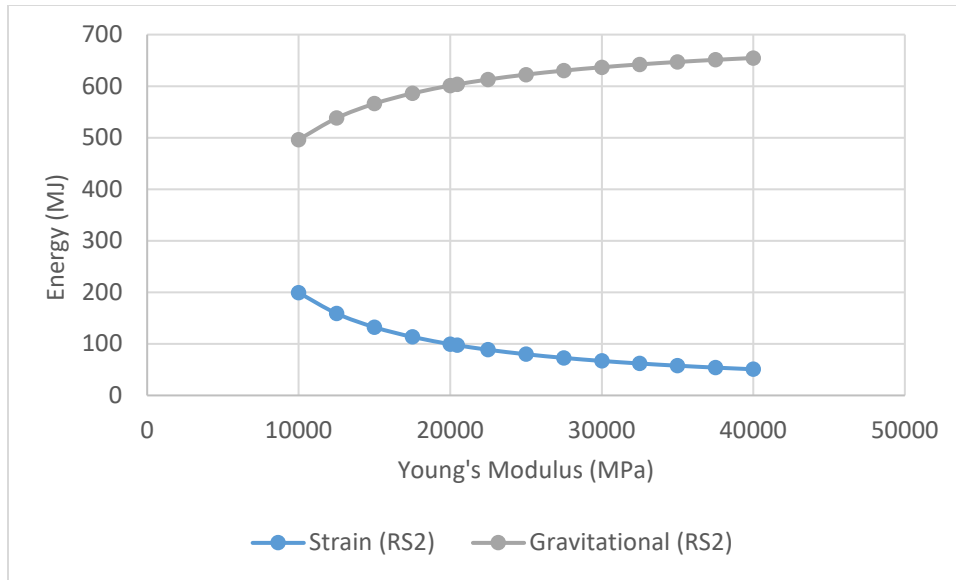
Figure 5.5: Comparison of strain and gravitational energy at various elastic moduli
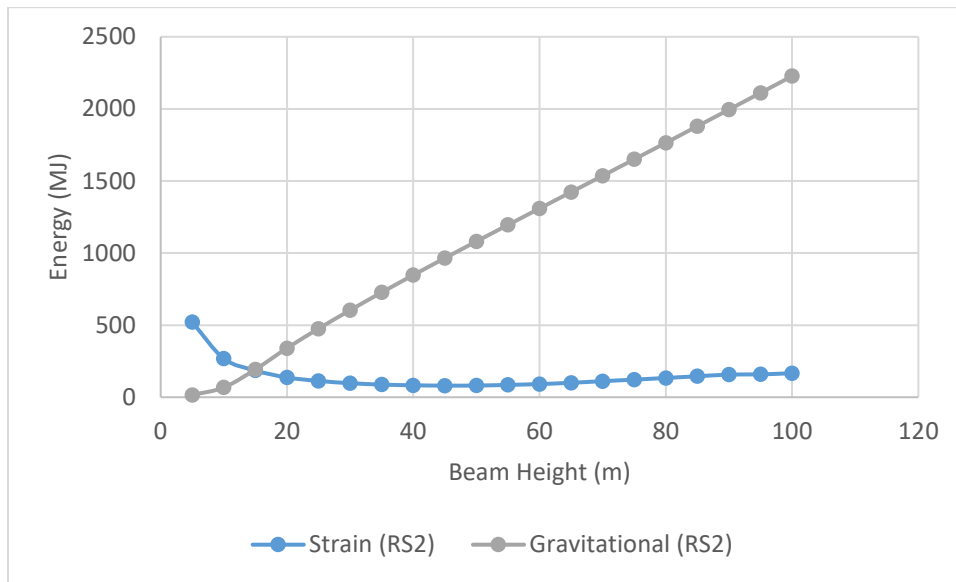
Figure 5.6: Comparison of strain and gravitational energy at various beam heights

For most cases, the gravitational energy is greater than the strain energy, indicating that gravitational potential energy is the main driving factor in the release of seismic energy. However, as the beam thickness decreases below 15 m, strain energy is greater than gravitational, indicating that strain energy has more effect at low beam heights. When the beam is at its highest flexure due to a thin beam, the energy stored due to deformation of the beam is higher than the energy due to the beam falling. At this point, the beam is at its highest level of deflection, so it has the lowest distance left to fall and the highest

32

deflection, and has the least weight, both factors decreasing gravitational energy and increasing strain energy.

5.2   Seismic Magnitude

The magnitude of seismic energy that is released into the mine workings when the longwall roof beam caves is calculated using equation 3.11.

5.2.1   Initial analysis

The magnitude of the seismic energy resulting from each the strain and gravitational energy determined using RS2, as well as the total energy released as a result of the beam falling for varying beam heights is shown in Figure 5.7. Beam width is 1 m, unsupported length is 330 m, and drop height is 3m.
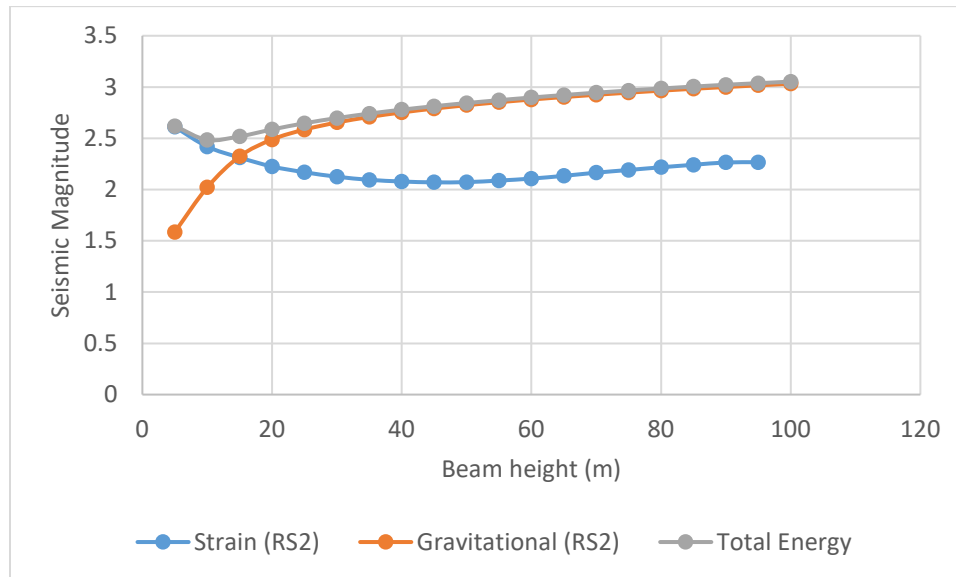
Figure 5.7: Seismic magnitude of strain, gravitational, and total energy from 1 m beam

Because seismic magnitude is calculated on a log scale, the greater magnitude energy is the driver for the resulting seismic energy. As the gravitational energy is greater in magnitude for the majority of the curve, as shown in Figure 5.6, the total seismic magnitude follows closely to the gravitational energy curve past 25 m. For low beam heights, the strain energy is the main driving factor for total energy, so the seismic magnitude follows the strain curve. The same analysis is conducted for a 10 m wide beam, shown in Figure 5.8. Beam unsupported length is 330 m, and drop height is 3m.

33
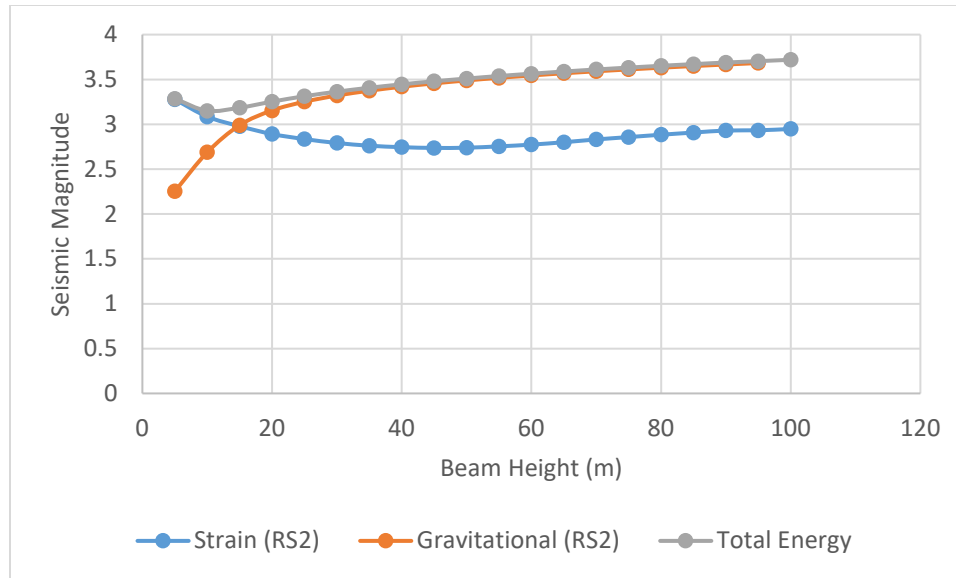
Figure 5.8: Seismic magnitude of strain, gravitational, and total energy from 10 m beam

The seismic magnitudes of a 1 m wide beam and a 10 m wide beam are compared in Figure 5.9.
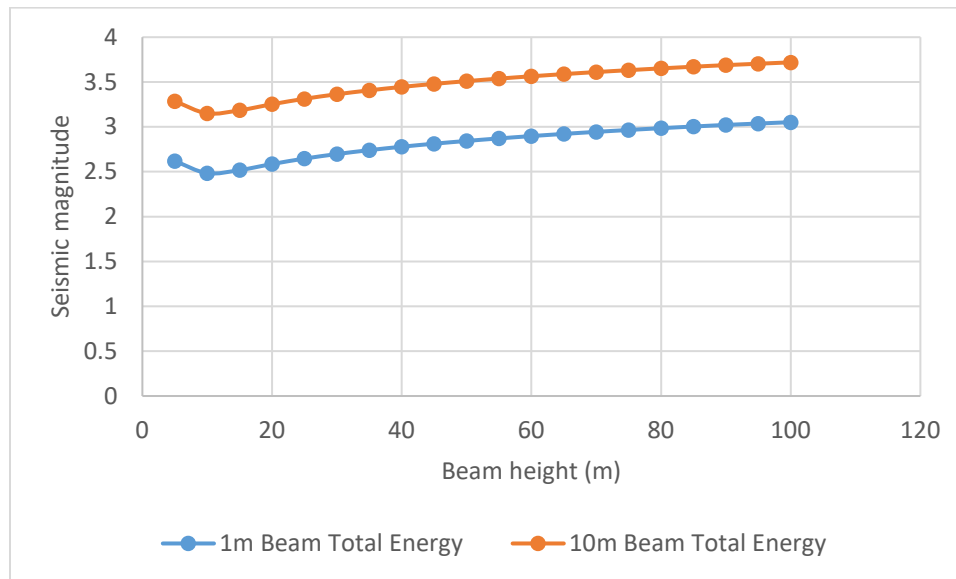
Figure 5.9: Seismic magnitude of total energy from 1 m and 10 m beams

The seismic magnitude of the 10 m beam caving is consistently greater than that of the 1 m wide beam. The greater weight with which to release energy upon falling and capability to store strain energy in the beam deformation allows the wider beam to release more energy than the 1 m beam. However, the increase in seismic energy is less than 10 times that of the 1 m beam, as the values for seismic energy are less than 1 greater than the

1 m beam values. The curves are parallel to each other, indicating that they follow the same pattern of high strain energy at low beam heights, and higher gravitational energy at high beam heights, shown also in Figure 5.8.

5.2.2   Refined analysis with swelling factor

Upon fracturing, rock increases in volume by its swelling factor. In the case of the fracture of longwall beams, this means that the distance the beam falls is reduced by the height taken up by the swelling of fractured material. Furthermore, the beam is not necessarily directly over the excavated panel. There can be other bedding units between the excavated coal and the strong beam, increasing the height at which the beam falls. With this information, the drop height can be better refined.

5.2.2.1 Drop height

The height at which the beam drops is a crucial factor in the calculation of energy, as drop height directly affects the gravitational energy released. In the previous analysis, it is assumed that the sandstone beam is directly over the coal seam, as shown in Figure 5.10. In this case, the sandstone will drop the height of the coal seam when it caves. However, there is another case where the sandstone beam is higher than the top of the coal seam, shown in Figure 5.11. In this case, there are additional strata between the coal and the strong beam, raising the height the beam will fall. In addition, the additional strata will fail and fill the void space below the beam, increasing in volume by a swelling factor. This then reduces the height that the beam will drop. The drop height is calculated using equation 5.1.

Figure 5.10: Beam directly over coal seam

Figure 5.11: Beam higher than top of coal seam due to additional strata

$$drop\ height = mining\ height$$
$$+ (distance\ above\ seam * swelling\ factor) \qquad 5.1$$
$$- beam\ deflection$$

The drop height will therefore change as the distance above the seam and swelling factors change, as shown in Figure 5.12. The total drop height calculated using equation 5.1, assuming a swelling factor of 1.2 and a deflection of 0.
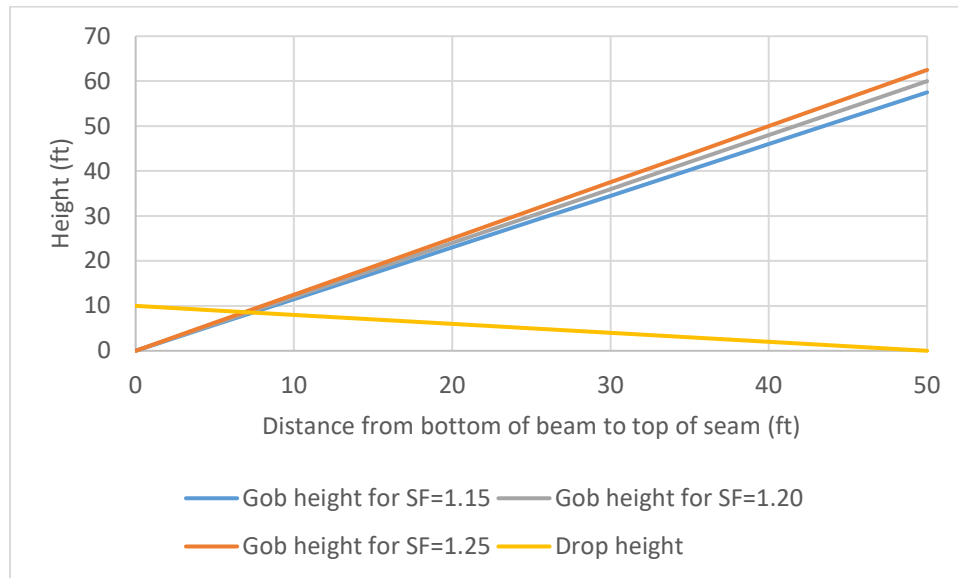
Figure 5.12: Void space for varying beam heights over seam and swell factors (SF)

As gob increases sharply, the drop height decreases more gradually. This is because the distance above the seam is increasing but is gradually being filled until the entire opening is filled with gob at 50 ft separating the beam from the mined opening.

Based on data provided by *Seismic magnitudes and frequencies at Buchanan Mine* (2022), the drop height varies from 1-8 ft. A value of 7 ft (2.1 m) is used for this analysis.

5.2.2.2 Back-calculating beam width

Using this analysis, the seismic energy released can be used to estimate the width of the beam that fractured in the mine. The sum of the gravitational and strain energy for various beam heights and widths from numerical models are converted to seismic magnitude, as shown in Figure 5.13. Here, the beam dimensions are adjusted to match the

data provided by Buchanan Mine. Beam unsupported length is 686 ft (209 m), and drop height is 7 ft (2.1 m).
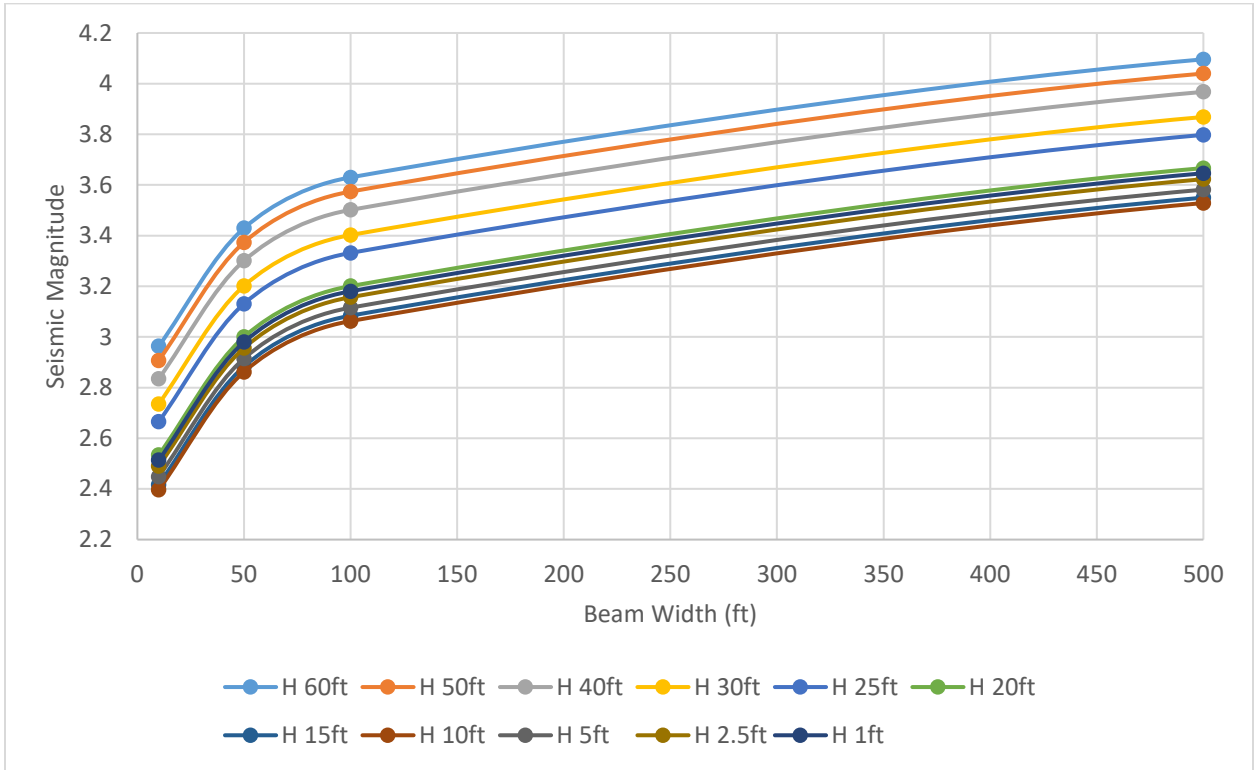
Figure 5.13: Seismic magnitude based on total energy for various beam widths and heights

As the beam width increases, seismic magnitude increases for all curves. The increase in beam width increases the weight of beam that falls, increasing the gravitational energy released by the mine. Also, increasing beam heights also causes an increase in seismic magnitude, similarly to the analysis shown in Figure 5.7.

This chart could potentially be used by a mining operation to estimate the width of the beam that fractured. Given the seismic magnitude of the energy released and the geologic report of the height of the beam, the width of the beam may be determined.

5.2.2.3 Back calculating drop height

A secondary analysis is done to determine the drop height of a beam, given beam dimensions and the resultant seismic magnitude. The drop height was varied from 4-8 ft for beams 10 ft wide and 10-25 ft high. The analysis is shown in Figure 5.14.
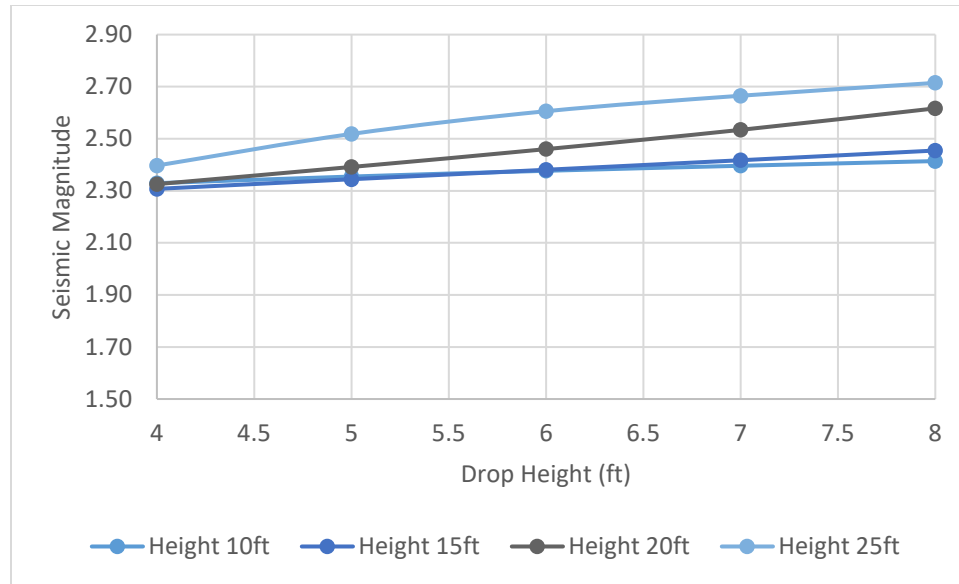
Figure 5.14: Seismic magnitude of total energy for various beam drop heights

Increasing drop height and beam height both cause an increase in seismic magnitude. Increasing drop height allows for a higher gravitational energy to be released upon beam caving, indicating an increase in seismic magnitude.

The lines for varying beam heights form an envelope of potential seismic magnitudes. The change in seismic magnitude increases with each additional 5 ft increase in beam height, indicating that the seismic magnitude will continue to increase with increasing beam height. This follows the same pattern displayed in Figure 5.7, as the beam increases in weight, the gravitational energy will cause the seismic magnitude to continue to increase.

This chart could potentially be used by a mining operation to estimate the drop height of the beam that fractured. Given the seismic magnitude of the energy released and the geologic report of the height and width of the beam, the drop height may be determined.

5.2.3   Seismic magnitudes of Buchanan Mine

The magnitude and frequency of earthquakes at Buchanan mine, provided *Seismic magnitudes and frequencies at Buchanan Mine* (2022), are shown in Figure 5.15. Most seismic events are below magnitude 1. There are several events above magnitude 2, which are likely due to beam breaking.

There are also many events of negative seismic value. In equation 3.11, there is a 11.8 term added to the equation. Because of this, if the earthquake has a small amount of energy, the log term may be less than 11.8, resulting in a negative value for seismic magnitude. Thus, the negative magnitudes of seismic events represent small events.
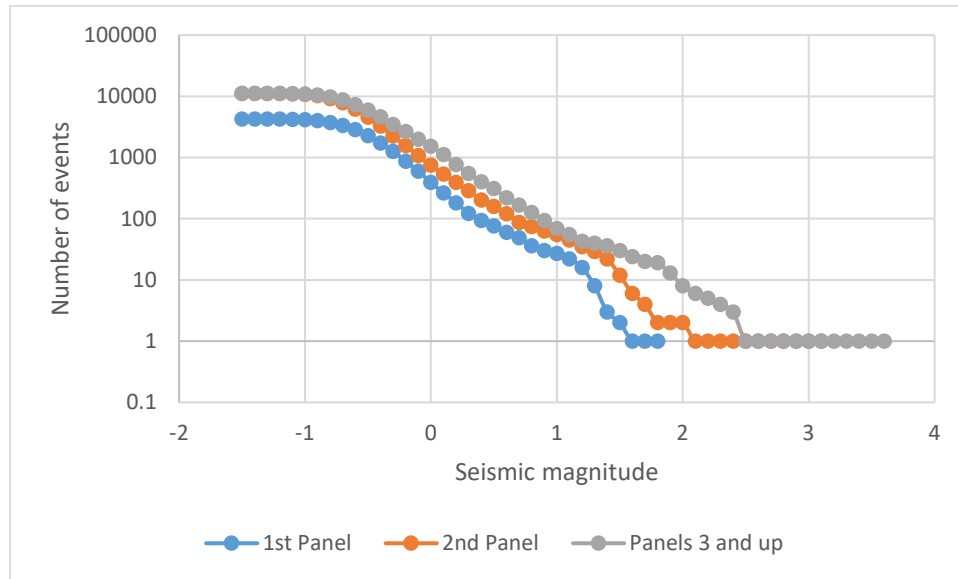
Figure 5.15: Frequencies of seismic events at Buchanan Mine (2022)

The Buchanan mine has had many low-magnitude seismic events, as well as several individual events above magnitude 2. A greater number of events have occurred above or around the second panel of a district than the first panel in the same district, and the second panel has several events above magnitude 2. An example of panel layout in plan view is shown in Figure 5.16. Panels refer to blocks of longwall mining areas and are numbered in the order mined. Districts consisting of several panels are surrounded on either side by barrier pillars.
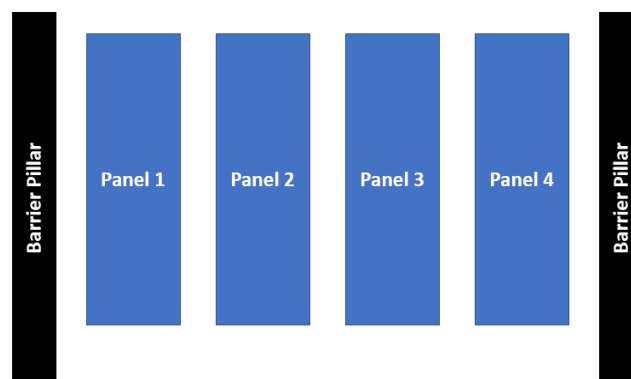
Figure 5.16: Plan view of panel layout in districts

Beams may fracture between adjacent panels, resulting in unconnected beams over separate panels. A description of this failure mode is shown in cross-section in Figure 5.17.
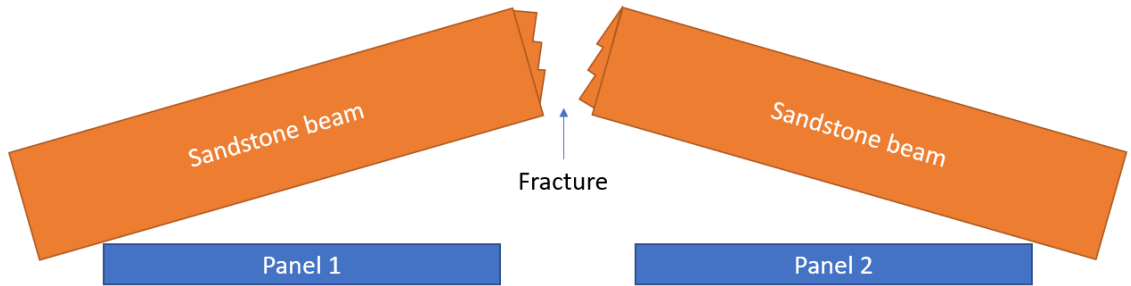
Figure 5.17: Potential beam fracture mode between adjacent panels

To verify the analysis performed above, the drop height and seismic magnitude of the data provided by *Seismic magnitudes and frequencies at Buchanan Mine* (2022) for specific seismic events above magnitude 2 are plotted with the results shown in Figure 5.14. The comparison is shown in Figure 5.18. Each point of the Buchanan mine data represents an individual event at a specific mined area. For each point, geologic data has been interpolated based on geologic models of the mine. The x- and y-coordinates of the events are triangulated from the seismic monitoring system, however the z-coordinate is difficult to determine using this method.
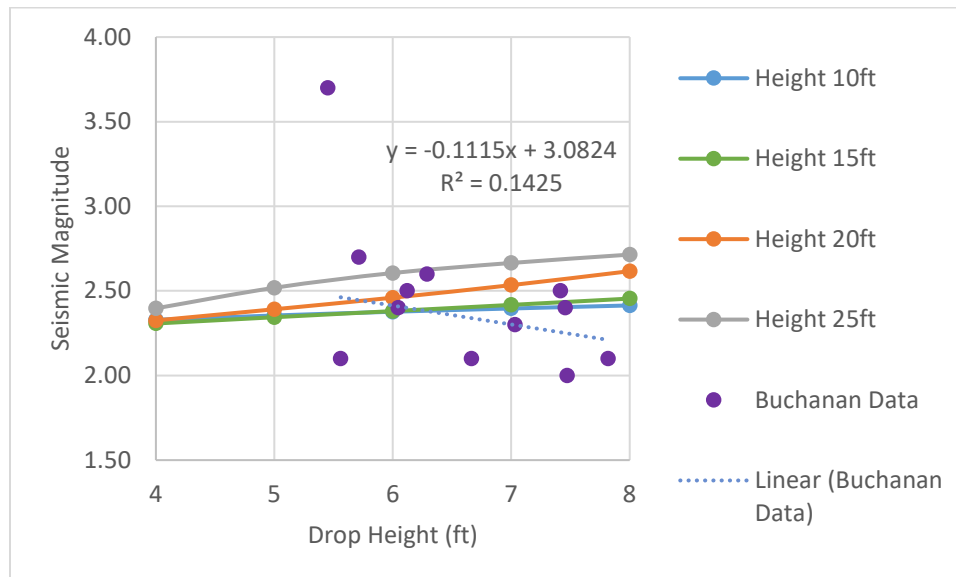
Figure 5.18: Predicted versus actual seismic magnitude and drop height

The prediction lines form an envelope for various beam heights at beam widths of 10 ft. As beam width is difficult to interpolate from mine data, this provides a range of seismic magnitudes that could result from a specified beam width.

A trendline is plotted for the mine data, excluding the outlier at a drop height of 5.5 ft and seismic magnitude of 3.7. The trendline shows a negative slope, indicating a decrease in seismic magnitude as drop height increases. This may be due to the presence of fractured material below the beam dissipating gravitational energy. Increasing drop height indicates an increase in gob below the beam, allowing for more energy to dissipate into the fractured material than is released directly into the mine operations. Lower drop heights indicate less gob and thus a solid surface that propagates seismic energy.

The point with a drop height of 5.5 ft and seismic magnitude of 3.7 is significantly above the envelope shown by the plotted lines. This indicates that the beam height or width may be significantly above those predicted.

6.1   Conclusions

The strain and gravitational energy released by a beam in a longwall roof can be modelled by a two-dimensional numerical model that matches the analytical equations. From this, the seismic magnitude of the energy released can be determined for varying beam geometries and properties.

Gravitational energy is greater in magnitude than strain energy for all cases, except for when the beam height is less than 15 m. Thus, gravitational energy is the driving factor in most cases of energy release due to beam caving.

The predicted seismic magnitudes for varying beam drop heights are compared to actual mine data for the Buchanan Mine, provided in *Seismic magnitudes and frequencies at Buchanan Mine* (2022). It is shown that the seismic magnitude decreases with increasing drop height, rather than increasing. This indicates that the energy released into the mine is impacted by the presence of gob below the beam. An increase in fractured material below the beam allows gravitational energy to dissipate into the gob without being released into the surrounding area. Lower drop heights indicate less gob below the beam and thus a solid surface onto which the beam can fall. This solid surface propagates more of the seismic energy to the surrounding areas, increasing the seismic magnitude measured.

6.2   Recommendations

Further research is recommended to look at the impact of various properties on the seismicity released to the mining operation.

6.2.1   Nominal extraction height

The analysis performed assumes a nominal extraction height of 3 m (9.8 ft). Due to variations in seam height, the actual extraction height may vary from 8-12 ft. The extraction height directly affects the gravitational energy released upon strata caving. In future analysis, the variation in seam height should be accounted for.

6.2.2 Portion of energy transferred to seismicity

It is assumed in this analysis that 100% of the gravitational and strain energy are transferred to seismic magnitude upon beam caving. Some strain energy is dissipated in the form of heat and fracturing of solid material. Furthermore, the presence of gob allows gravitational energy of the falling beam to be partially dissipated before it spreads to the surrounding mine workings. Further work may be done to study the amount of strain energy and gravitational energy that is transferred to seismicity.

6.2.3 Three-dimensional model

The analysis is performed using a two-dimensional modelling software, RS2. Additional analysis could be done using a three-dimensional model of the longwall roof panel to better model the three-dimensional stress state on the roof beams.

6.2.4 Investigate RS2 field stress options

The menu provided by RS2 to model overburden as a field stress, shown in Figure 4.5, provides results that differ greatly from those of modelling the entire overburden. Further investigation into the calculations and impact of the RS2 field stress options is recommended.

REFERENCES

Alber, M., Fritschen, R., Bischoff, M., & Meier, T. (2008). Rock mechanical investigations of seismic events in a deep longwall coal mine. *International Journal of Rock Mechanics & Mining Sciences*, *46*, 408-420. https://doi.org/10.1016/j.ijrmms.2008.07.014

Beer, F. P., Jr., E. R. J., DeWolf, J. T., & Mazurek, D. F. (2015). *Mechanics of materials* (7th ed.). McGraw-Hill Education.

Choi, D. S. (1990). Improved source location and evaluation of seismic events over a deep coal mine, 9th International Conference on Ground Control in Mining, Morgantown, West Virginia.

Díaz-Mora, F., & González-Fallas, A. (2022). Energy harvesting from seismic waves for electricity production, International Conference on Energy and Green Computing, Virtual.

Esterhuizen, E., Mark, C., & Murphy, M. M. (2010). Numerical model calibration for simulating coal pillars, gob and overburden response, 29th International Conference on Ground Control in Mining, Morgantown, West Virginia, July 27-29.

Goode, C., Zona, A., & Campoli, A. (1984). Causes and control of coal mine bumps, 15th Annual Institute on Coal Mining Health, Safety and Research.

Gutenberg, B. (1945). Amplitudes of surface waves and magnitudes of shallow earthquakes. *Bulletin of the Seismological Society of America*, *35*(1), 3-12. https://doi.org/https://doi.org/10.1785/BSSA0350010003

Haramy, K. I., Kneialey, R., & McDonnell, J. P. (1987). Longwall face bursts and inadequate caving: A case study, 6th International Conference on Ground Control in Mining, Morgantown, West Virginia, June 9-11.

Hasegawa, H. S., Wetmiller, R. J., & Gendzwill, D. J. (1989). Induced seismicity in mines in Canada-An overview. *PAGEOPH*, *129*.

Hayes, G., & Wald, D. *Earthquake magnitude, energy release, and shaking intensity*. U.S. Department of the Interior. https://www.usgs.gov/programs/earthquake-hazards/earthquake-magnitude-energy-release-and-shaking-intensity

Iannacchione, A. T., & DeMarco, M. J. (1992). Optimum mine designs to minimize coal bumps: a review of past and present US practices. In *New Technology in Mining Health and Safety*. Society for Mining, Metallurgy, and Exploration.

Iannacchione, A. T., Esterhuizen, G. S., Bajpayee, T. S., Swanson, P. L., & Chapman, M. C. (2005). Characteristics of mining-induced seismicity associated with roof falls and roof caving events, 40th US Symposium on Rock Mechanics.

Logan, D. L. (2022). *A first course in the finite element method* (6th ed.). Cengage Learning.

Luxbacher, K., Westman, E., & Swanson, P. (1994). Time-lapse tomography of a longwall panel: A comparison of location schemes, 26th International Conference on Ground Control in Mining, Morgantown, West Virginia, August 2-4.

Okal, E. A. (2019). Energy and magnitude: A historical perspective. *Pure and Applied Geophysics*, *176*, 3815–3849. https://doi.org/10.1007/s00024-018-1994-7

Panza, G., Kossobokov, V. G., Peresan, A., & Nekrasova, A. (2014). Chapter 12 - Why are the standard probabilistic methods of estimating seismic hazard and risks too often

wrong. In J. F. Shroder & M. Wyss (Eds.), *Earthquake Hazard, Risk and Disasters* (pp. 309-357). Academic Press. https://doi.org/https://doi.org/10.1016/B978-0-12-394848-9.00012-2

Pariseau, W. G. (2017). Comparison of underground coal and trona mine seismicity, Society of Mining, Metallurgy, and Exploration, Denver, Colorado, Feb. 19-22.

RS2. In. (2021). Rocscience. https://www.rocscience.com/software/rs2

Seismic magnitudes and frequencies at Buchanan Mine. (2022). Coronado Global Resources.

Serway, R. A., & Jewett, J. W. (2018). *Physics for scientists and engineers*. Cengage learning.

Van Dyke, M. A., Su, W. H., & Wickline, J. (2018). Evaluation of seismic potential in a longwall mine with massive sandstone roof under deep overburden, 36th International Conference on Ground Control in Mining, Morgantown, WV.

Wu, X., & Karfakis, M. G. (1993). Mathematical modeling of strong roof beds in longwall mining, 12th International Conference on Ground Control in Mining, Morgantown, West Virginia, August 3-5.

VITA

Caroline Gerwig

- Educational institutions attended:
  - University of Kentucky, Bachelor of Science in Mining Engineering
  - Graduated undergraduate degree Summa Cum Laude
- Professional positions held:
  - Mine planning intern with Nevada Gold Mines
  - Mining engineering intern with RESPEC
  - Mining engineering intern with Martin Marietta
- Scholastic and professional honors:
  - Engineer-in-training (EIT) due to passing Fundamentals in Engineering (FE) exam
  - Mu Nu Gamma Mining Engineering Honors Society
  - Tau Beta Pi Engineering Honors Society
  - Dean's List 2017-2021
  - Academic Excellence Award for undergraduate mining engineering degree
  - Outstanding Senior Award for undergraduate mining engineering degree
- Professional publication:
  - Gerwig, C., Androulakis, V., Agioutantis, Z. "Strain energy considerations related to strata failure during caving operations." International Conference on Ground Control Mining, Canonsburg, PA, July 26-28, 2022. Paper submitted, peer reviewed, presented at ICGCM.